



**HAL**  
open science

## Heterogeneity of neuroblastoma cell identity defined by transcriptional circuitries

Valentina Boeva, Caroline Louis-Brennetot, Agathe Peltier, Simon Durand, Cecile Pierre-Eugene, Virginie Raynal, Heather Etchevers, Sophie Thomas, Alban Lermine, Estelle Daudigeos-Dubus, et al.

► **To cite this version:**

Valentina Boeva, Caroline Louis-Brennetot, Agathe Peltier, Simon Durand, Cecile Pierre-Eugene, et al.. Heterogeneity of neuroblastoma cell identity defined by transcriptional circuitries. *Nature Genetics*, 2017, 49 (9), pp.1408-1413. 10.1038/ng.3921 . hal-01741718

**HAL Id: hal-01741718**

**<https://hal.science/hal-01741718v1>**

Submitted on 26 Mar 2018

**HAL** is a multi-disciplinary open access archive for the deposit and dissemination of scientific research documents, whether they are published or not. The documents may come from teaching and research institutions in France or abroad, or from public or private research centers.

L'archive ouverte pluridisciplinaire **HAL**, est destinée au dépôt et à la diffusion de documents scientifiques de niveau recherche, publiés ou non, émanant des établissements d'enseignement et de recherche français ou étrangers, des laboratoires publics ou privés.

# Heterogeneity of neuroblastoma cell identity revealed by transcriptional circuitries

Authors: Valentina Boeva<sup>1,2,\*</sup>, Caroline Louis-Brennetot<sup>3</sup>, Agathe Peltier<sup>3</sup>, Simon Durand<sup>3</sup>, Cécile Pierre-Eugène<sup>3</sup>, Virginie Raynal<sup>3,4</sup>, Heather Etchevers<sup>5</sup>, Sophie Thomas<sup>6</sup>, Alban Lermine<sup>1</sup>, Estelle Daudigeos-Dubus<sup>7</sup>, Birgit Georger<sup>7</sup>, Martin F. Orth<sup>8</sup>, Thomas G. P. Grünewald<sup>8</sup>, Elise Diaz<sup>9,10</sup>, Bertrand Ducos<sup>9,10,11</sup>, Didier Surdez<sup>3</sup>, Angel M. Carcaboso<sup>12</sup>, Irina Medvedeva<sup>2</sup>, Thomas Deller<sup>13</sup>, Valérie Combaret<sup>14</sup>, Eve Lapouble<sup>15</sup>, Gaelle Pierron<sup>15</sup>, Sandrine Grossetête-Lalami<sup>3</sup>, Sylvain Baulande<sup>4</sup>, Gudrun Schleiermacher<sup>3,16,17</sup>, Emmanuel Barillot<sup>1</sup>, Hermann Rohrer<sup>13</sup>, Olivier Delattre<sup>3</sup>, and Isabelle Janoueix-Lerosey<sup>3,\*</sup>

\* Corresponding authors

## Affiliations

<sup>1</sup>Institut Curie, PSL Research University, Inserm U900, Mines-ParisTech, F-75005, Paris, France.

<sup>2</sup>Institut Cochin, Inserm U1016, CNRS UMR 8104, University Paris Descartes UMR-S1016, F-75014, Paris, France.

<sup>3</sup>Institut Curie, PSL Research University, Inserm U830, F-75005, Paris, France.

<sup>4</sup>Institut Curie Genomics of Excellence (ICGex) Platform, Institut Curie Research Center, F-75005, Paris, France.

<sup>5</sup>Aix Marseille Univ, Inserm, GMGF, UMR S910, F-13005, Marseille, France.

<sup>6</sup>Inserm U1163, Laboratory of Embryology and Genetics of Congenital Malformations, Paris Descartes - Sorbonne Paris Cité University, Imagine Institute, F-75015 Paris, France.

<sup>7</sup>Vectorology and Anticancer Therapies, UMR 8203, CNRS, Univ. Paris-Sud, Gustave Roussy, Université Paris-Saclay, F-94805, Villejuif, France.

<sup>8</sup>Max-Eder Research Group for Pediatric Sarcoma Biology, Institute of Pathology, LMU Munich, Thalkirchner Str. 36, 80337 Munich, Germany.

<sup>9</sup>High Throughput qPCR facility, IBENS, PSL Research University, 46 rue d'Ulm, F-75005,

30 Paris, France.

31 <sup>10</sup>LPS-ENS, UPMC, Université Denis Diderot, CNRS UMR 8550, PSL 24 rue Lhomond, F-  
32 75005, Paris, France.

33 <sup>11</sup>Laser Microdissection Facility, CIRB Collège de France, Place Marcellin Berthelot, F-75005,  
34 Paris, France.

35 <sup>12</sup>Institut de Recerca Sant Joan de Deu, 08950 Barcelona, Spain.

36 <sup>13</sup>Institute for Clinical Neuroanatomy, Goethe University, D-60590, Frankfurt/M, Germany.

37 <sup>14</sup>Centre Léon Bérard, Laboratoire de Recherche Translationnelle, Lyon, France.

38 <sup>15</sup>Institut Curie, Unité de Génétique Somatique, F-75005, Paris, France.

39 <sup>16</sup>Laboratory RTOP (Recherche Translationnelle en Oncologie Pédiatrique), laboratoire  
40 "Gilles Thomas", Institut Curie, F-75005, Paris, France.

41 <sup>17</sup>Department of translational research, Institut Curie, F-75005, Paris, France.

42

43

44 Neuroblastoma is a tumor of the peripheral sympathetic nervous system<sup>1</sup>, derived from  
45 multipotent neural crest cells (NCCs). To define Core Regulatory Circuitries (CRCs) controlling  
46 the gene expression program of neuroblastoma, we established and analyzed the neuroblastoma  
47 super-enhancer landscape. We discovered three types of identity in neuroblastoma cell lines: a  
48 sympathetic noradrenergic identity defined by a CRC module including the PHOX2B, HAND2  
49 and GATA3 transcription factors (TFs); an NCC-like identity, driven by a CRC module  
50 containing AP-1 family TFs; a mixed type further deconvoluted at the single cell level.  
51 Treatment of the mixed type with chemotherapeutic agents resulted in enrichment of NCC-like  
52 cells. The noradrenergic module was validated by ChIP-seq. Functional studies demonstrated  
53 dependency of neuroblastoma with noradrenergic identity on PHOX2B, evocative of lineage  
54 addiction. Most neuroblastoma primary tumors express TFs from the noradrenergic and NCC-  
55 like modules. Our data demonstrate a novel aspect of tumor heterogeneity relevant for  
56 neuroblastoma treatment strategies.

57

58 **Keywords:** neuroblastoma, neural crest cells, ChIP-seq, super-enhancers, core regulatory  
59 circuitries, transcription factors, cell proliferation

60

61 Nearly one in six patients who die of a childhood cancer had a neuroblastoma, a tumor of  
62 the peripheral sympathetic nervous system<sup>1</sup>. Several genes including *MYCN*<sup>2</sup>, *ALK*<sup>3-6</sup> and  
63 *TERT*<sup>7,8</sup> have been shown to act as major drivers of neuroblastoma oncogenesis. In this work, we  
64 have determined the core transcriptional regulatory circuitries (CRCs)<sup>9</sup> that govern the gene  
65 expression program of neuroblastoma. CRCs, which can be defined by super-enhancer (SE)  
66 mapping of H3K27 acetylation mark (H3K27ac) and further sequence motif analysis, provide  
67 integrative information about cell identity<sup>9,10</sup>.

68 We examined a panel of twenty-five neuroblastoma cell lines (Table S1) and two primary  
69 human neural crest cell (hNCC) lines<sup>11</sup>. SEs were defined by the ROSE algorithm<sup>12</sup> modified to  
70 account for copy number changes. Principal Component Analysis (PCA), based on scores of SEs  
71 identified in at least two neuroblastoma cell lines or in both hNCC lines (n=5975) revealed two  
72 distinct groups (Figure 1a): group I with 18 neuroblastoma cell lines and group II comprising the  
73 GIMEN, SH-EP and *GICAN* neuroblastoma cell lines. Group II closely resembled the hNCC  
74 lines in this analysis. Four neuroblastoma cell lines occupied an intermediate position between  
75 groups I and II. These included the phenotypically heterogeneous SK-N-SH cell line whereas its  
76 sub-clones, SH-SY5Y and SH-EP, were included in groups I and II, respectively. This result is  
77 consistent with SH-SY5Y cells displaying neurite-like processes and expressing noradrenergic  
78 biosynthetic enzymes TH and DBH (“N” phenotype), and SH-EP cells exhibiting a substrate-  
79 adherent “S” phenotype without expression of TH and DBH<sup>13</sup>. We also profiled the SE  
80 landscape of six patient-derived xenografts (PDXs), five of them with *MYCN* amplification  
81 (Table S2). All PDXs clustered with group I when included in the PCA (Figure 1a).

82 SEs were then sorted according to the median H3K27ac signal for each group (Figure 1b  
83 and 1c, respectively; Table S3). In group I, the strongest SEs comprise a set of transcription  
84 factor (TF) loci including *HAND2*, *PHOX2A/PHOX2B* and *GATA2/GATA3* and the *ALK*  
85 oncogene locus (Figure 1b, 1d, 1e, Figures S1 and S2). These findings are consistent with  
86 previous SE data on a few neuroblastoma cell lines<sup>14,15</sup>. *PHOX2B*, *HAND2*, and *GATA3* are  
87 known to participate in a complex TF network controlling normal sympathetic neuron  
88 specification and differentiation<sup>16,17</sup>. Recurrent SEs in these TFs therefore appear to be a  
89 hallmark of sympathetic cell identity. Most SEs of group II overlapped with SEs of hNCC lines  
90 (Figure 1c), consistent with the results of the PCA analysis.

91 Our analysis found *MYCN* SEs for 10 out of 18 cell lines of group I, with or without

92 *MYCN* amplification, and 3 PDX (Figure S3). No groups linked to the *MYCN* or *ALK* status were  
93 revealed in the PCA. Furthermore, supervised analysis of SE scores did not indicate SEs  
94 associated with *MYCN* amplification or *ALK* mutations (Tables S4 and S5). Cell lines with a  
95 *PHOX2B* mutation were observed in group I (SH-SY5Y), group II (SH-EP) or in the  
96 intermediate group (SK-N-SH).

97 To detect driver TFs for groups I and II, we used i-cisTarget to find DNA sequence  
98 motifs enriched in the SEs with the highest score. For group I, this analysis identified a  
99 TAATYYAATTA binding motif common to several homeobox proteins, including PHOX2B  
100 and PHOX2A (Figure S4). During sympathetic nervous system development PHOX2B regulates  
101 PHOX2A expression<sup>18</sup>. Both TFs are highly expressed in most neuroblastoma cell lines and  
102 primary tumors (Figure S5). PHOX2B was undetectable at the transcript and protein level solely  
103 in the group II cell lines as well as in the hNCC lines, but was expressed in all other  
104 neuroblastoma cell lines (Figure 1f; Figure S6). There was a corresponding lack of SE at  
105 *PHOX2B* and no TH and DBH transcription in GIMEN, SH-EP and GICAN (Figure S7). I-  
106 cisTarget analysis showed enrichment in AP-1 motif in group II and in the hNCC lines (Figures  
107 S8 and S9). AP-1 is a heterodimer composed of FOS and JUN family members both of which are  
108 expressed in immature hNCC<sup>11</sup>. These results suggest that PHOX2B participates in the activity  
109 of neuroblastoma group I SEs while the AP-1 complex TFs influence the SE landscape of group  
110 II.

111 A CRC calling algorithm<sup>9,19</sup> identified PHOX2B as group I-specific CRC TF and FOSL1,  
112 FOSL2 and JUN for group II (Figure S10), consistent with our i-cisTarget results. We therefore  
113 searched for TFs predicted to be in a CRC either with PHOX2B or a FOS/JUN family member  
114 (Figure 1g). Cell lines showing an intermediate position in the PCA had a CRC that included  
115 several TFs of both PHOX2B-associated and FOS/JUN-associated sets. Most of TFs of the latter  
116 set are expressed in neural crest cells and/or mesenchymal neural crest derivatives. The CRCs of  
117 the six PDXs were highly similar to those of the group I cell lines (Figure 1g). As we  
118 documented that SE strength linearly correlated with gene expression (Figure S11), we used the  
119 latter to further define fully connected TF modules. This analysis revealed two main TF modules  
120 distinguishing groups I and II (Figure 1h). PHOX2B, GATA3 and HAND2 were present in  
121 module 1 whereas module 2 included FOSL1 and FOSL2. These modules were anti-correlated at  
122 the gene expression level. Western blot analysis confirmed the co-expression of several TFs in

123 group I or group II (Figure S12). Furthermore, single cell analysis showed that the SK-N-AS and  
124 SK-N-SH cell lines are heterogeneous and comprise cells expressing TFs of either module 1 or  
125 module 2 within the same population (Figure 1i, Figure S13, Table S6).

126 Taken together, these data demonstrate a novel type of heterogeneity in neuroblastoma  
127 cell lines and suggest that individual cells assume either a sympathetic noradrenergic identity,  
128 characterized by a CRC module including PHOX2B, HAND2 and GATA3, and subsequent  
129 expression of the enzymes TH and/or DBH; or an NCC-like identity, characterized by expression  
130 of a distinct module including FOS and JUN family members but lacking PHOX2B and  
131 noradrenergic marker expression. Both types of identity are observed in several heterogeneous  
132 cell lines. All cell lines with *MYCN* amplification except one (CHP-212) had a noradrenergic  
133 identity whereas cell lines without *MYCN* amplification displayed any of the three identities  
134 (Figure 1g).

135 To explore whether the different identity classes seen in neuroblastoma cell lines are also  
136 characteristic for neuroblastoma primary tumors, expression data from a large set of primary  
137 tumors (n=498; dataset GSE49711)<sup>20</sup> were studied. Correlations between expression of the TFs  
138 of each module identified in cell line CRCs were calculated for these primary tumors. We found  
139 strong positive correlations between PHOX2B, HAND2, and GATA3 of module 1 as well as  
140 between the TFs of the NCC-like module (Figure 2a). We also observed anti-correlations  
141 between PHOX2B, HAND2, and GATA3 on the one hand, and TFs of the NCC-like module on  
142 the other hand. These results therefore confirm the data obtained with cell lines and further  
143 define a PHOX2B/HAND2/GATA3 noradrenergic CRC module in primary neuroblastomas.  
144 Next, we used the average expression of the two modules to explore primary tumor identity. All  
145 but two tumors showed high expression of the noradrenergic module (Figure 2b). A continuum  
146 was observed between low to high values of the NCC-like module, suggesting heterogeneity of  
147 cell identity in primary tumors. The remaining two cases with low noradrenergic and high NCC-  
148 like module expression may correspond to rare cases with full NCC-like identity, as described  
149 for group II cell lines. Similar to the cell lines (Figure S14), lower expression of the NCC-like  
150 module was observed in the majority of *MYCN*-amplified tumors (two-sided Wilcoxon signed-  
151 rank test p-value  $1.01 \times 10^{-10}$ ). A role for *MYCN* in downregulation of genes from this module is  
152 consistent with its promotion of peripheral neuron differentiation from multipotent avian NCC<sup>21</sup>.

153 Next, expression of the NCC-like and noradrenergic modules was evaluated in a series of

154 10 diagnosis/relapse sample pairs<sup>22</sup>. Different patterns were observed between the two disease  
155 stages (Figure 2c). To address a possible link between heterogeneity of cell identity and  
156 treatment response, we investigated the effect of chemotherapy on the NCC-like SH-EP and  
157 noradrenergic SH-SY5Y cell lines. SH-EP cells were more resistant to the three agents used  
158 (Figure S15). Treatment of the parental SK-N-SH cell line with doxorubicin or cisplatin resulted  
159 in the respective decreased or increased expression of module 1 and 2 (Figure 2d). Enrichment of  
160 cells with an NCC-like identity thus correlates with better drug resistance. However, we cannot  
161 exclude that treatment may also induce transdifferentiation from noradrenergic to NCC-like  
162 identity. The observation that tumors at relapse are not systematically enriched in NCC-like cells  
163 supports the concept of plasticity in the reversion of cell identity. This may rely on a switch from  
164 adrenergic to NCC-like identity under chemotherapy and from NCC-like to noradrenergic after  
165 treatment. Altogether, these data underline the importance of targeting both types of cells during  
166 treatment.

167 Strong correlations between PHOX2B, HAND2 and GATA3 expression were observed  
168 both in cell lines and tumors. Phox2b directly binds Hand2 protein<sup>23</sup>, and Phox2b, Hand2 and  
169 Gata3 cross-regulate during sympathetic nervous system development<sup>16</sup>. We therefore performed  
170 ChIP-seq analysis for these TFs in the CLB-GA neuroblastoma cell line and identified binding  
171 motifs for PHOX2B, HAND2 (zinc finger TF) and GATA3 (bHLH leucine zipper TF) (Figure  
172 3a). Binding regions for all three TFs corresponded to the H3K27ac peaks in the *PHOX2B*,  
173 *GATA3*, *HAND2* and *ALK* SEs and also in the *MYCN* SE (Figure 3b and 3c, Figure S16). These  
174 results therefore confirm the biological existence of the noradrenergic module, showing that  
175 PHOX2B, HAND2 and GATA3 are SE-regulated and bind to the SEs of each other (Figure 3d).  
176 We next investigated the occupancy by these TFs of 4,336 SE regions predicted in at least two  
177 neuroblastoma cell lines. SE regions were ranked according to average SE score and intersection  
178 with TF binding sites was evaluated. Over 90% of the strong and recurrent neuroblastoma SEs  
179 were co-occupied by PHOX2B, HAND2 and GATA3 (Figure 3e). Additionally, positional  
180 binding analysis showed that HAND2, PHOX2B and GATA3 bind the same ~400 bp-long  
181 regions within active regulatory regions (Figure 3f). Altogether, our results demonstrate that  
182 PHOX2B, HAND2 and GATA3 are master TFs defining the SE landscape of neuroblastoma cell  
183 lines with a noradrenergic identity.

184 It has been demonstrated that cancer dependencies can be found among SE-marked

185 genes<sup>19,24</sup>. Although missense and frameshift *PHOX2B* mutations predispose to  
186 neuroblastoma<sup>25,26</sup>, its role in sporadic neuroblastoma remains poorly understood. Phox2b knock-  
187 out mice completely lack autonomic structures<sup>17</sup> whereas conditional knock-out leads to  
188 decreased neuroblast proliferation<sup>27</sup>. An effect of PHOX2B knockdown on neuroblastoma cell  
189 proliferation has been previously suggested<sup>28</sup>. To further document the consequence of PHOX2B  
190 knockdown on neuroblastoma growth, we generated a doxycycline-inducible anti-*PHOX2B*  
191 short-hairpin RNA (shRNA) expression system in noradrenergic CLB-GA and SH-SY5Y cells.  
192 Inducible decrease of PHOX2B protein (Figure 4a, 4c) resulted in significant inhibition of  
193 neuroblastoma cell growth (Figure 4b, 4d, Figure S17). Decreased expression of PHOX2B in  
194 CLB-GA cells also impaired tumor growth *in vivo* (Figure 4e and 4f, Figure S18). We then  
195 evaluated whether PHOX2B decrease was sufficient to change the noradrenergic identity of the  
196 CLB-GA and SH-SY5Y cell lines to an NCC-like identity. However, data obtained by RNA-seq  
197 and RT-q-PCR suggested that the residual level of PHOX2B was sufficient to maintain a  
198 noradrenergic identity (Figure S19). This observation is consistent with the noradrenergic  
199 identity of the CLB-PE cell line in which PHOX2B expression is low but detected at the protein  
200 and RNA levels (Figures 1f and S6).

201 We observed a reduction of proliferation upon HAND2 and GATA3 knockdown in  
202 several cell lines, consistently with previous data on GATA3 knockdown<sup>15</sup> (Figure S20). These  
203 results are in line with Hand2 and Gata3 controlling sympathetic neuroblast proliferation<sup>16</sup>.  
204 Neuroblastoma cells of noradrenergic identity therefore appear to be addicted to these key  
205 lineage TFs as well as to PHOX2B<sup>29</sup>.

206 In conclusion, our work provides fundamental insights into the transcriptomic and  
207 epigenomic landscape of neuroblastoma. Distinct TF networks predicate different tumor  
208 identities, corresponding to sympathetic noradrenergic or NCC-like identity. Most primary  
209 tumors comprise cells of both identities, revealing a novel aspect of tumor heterogeneity.  
210 Neuroblastoma treatment should benefit from specifically targeting both identities.

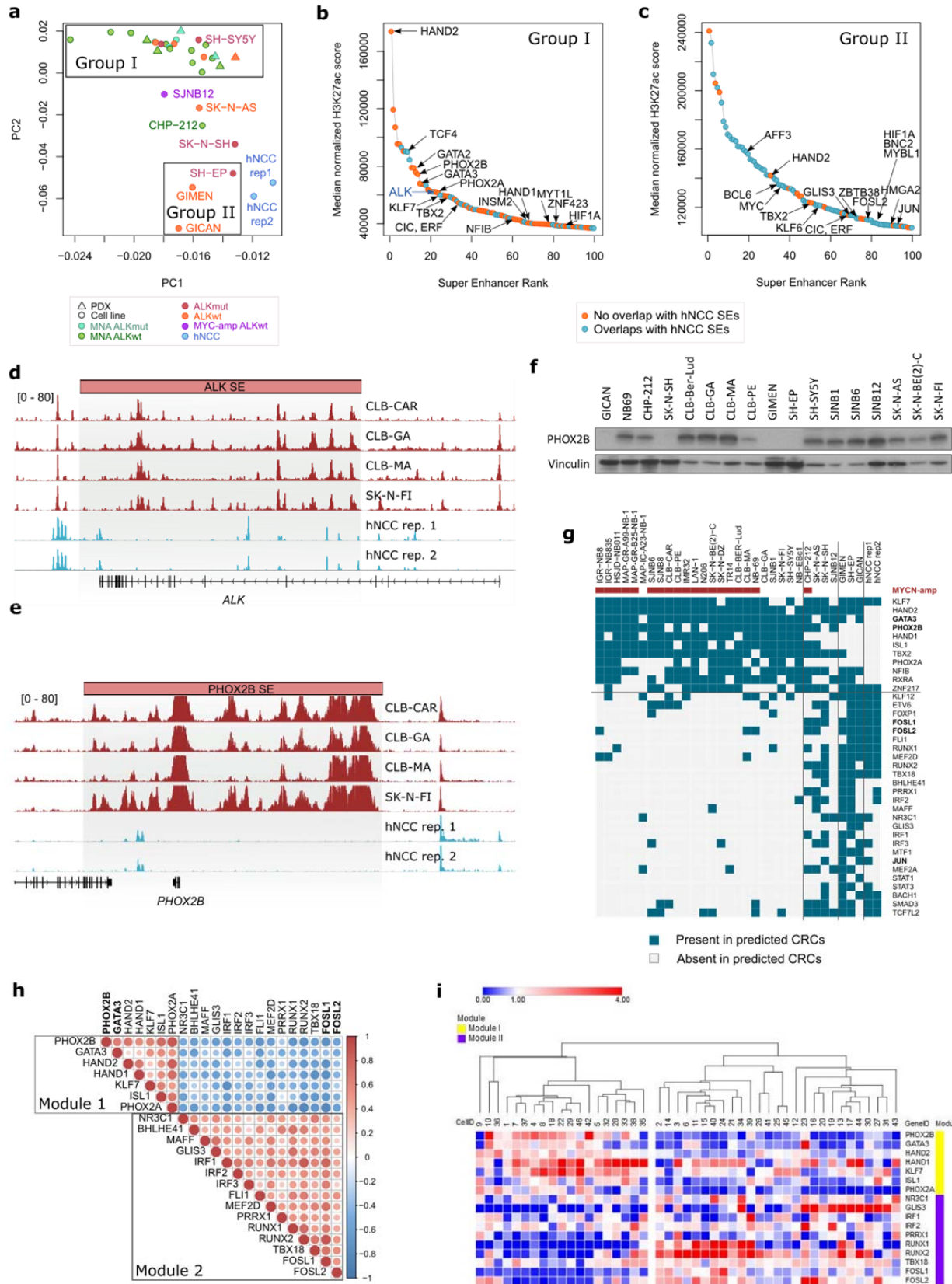
211

212

213

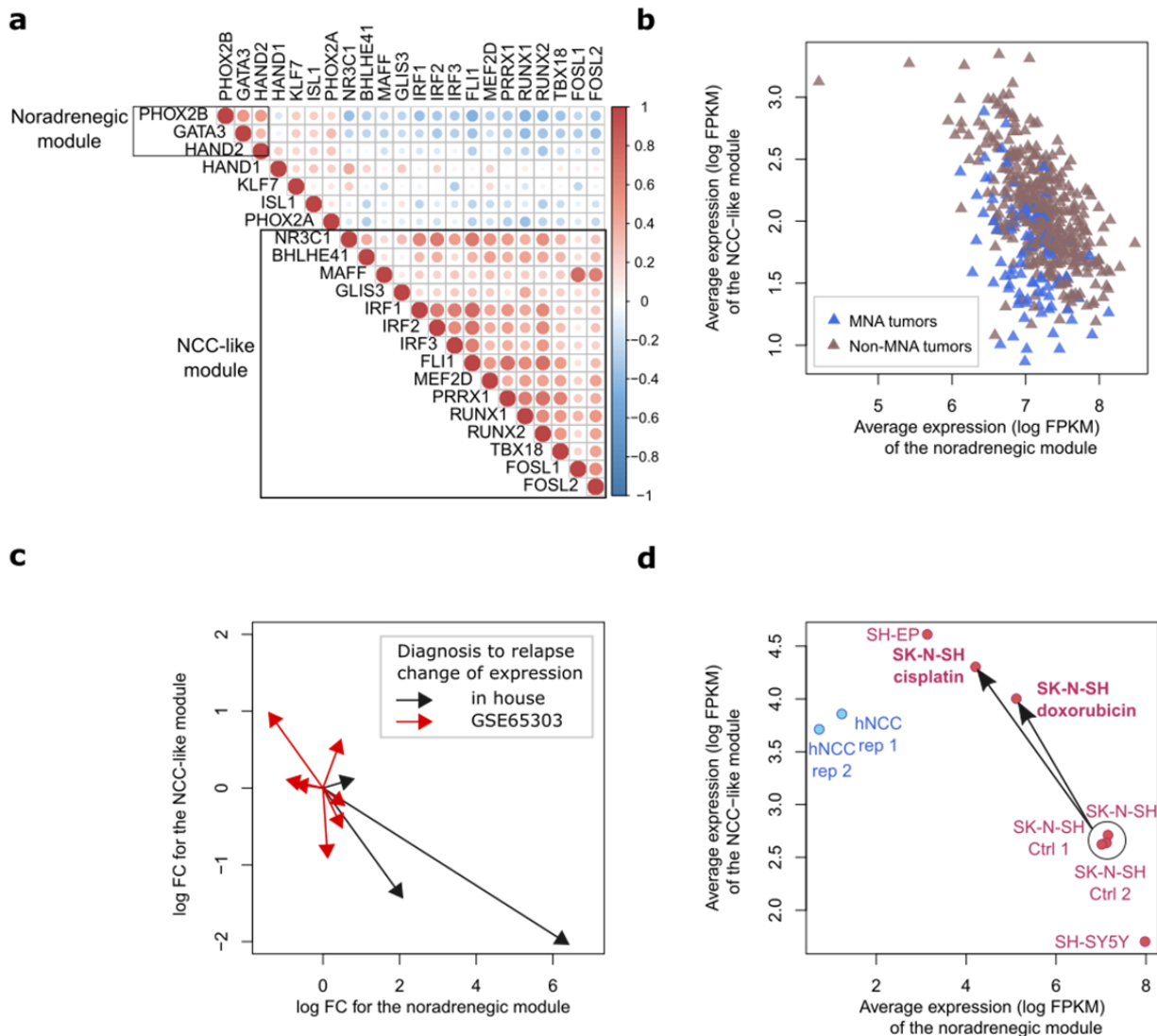
214





216 **Figure 1. SE landscape reveals various CRCs and identities in neuroblastoma cell lines. a,**  
217 Principal Component Analysis (PCA) based on neuroblastoma and hNCC SE log scores. MNA:  
218 MYCN amplification. **b, c,** Ranked plot for the 100 SEs with the highest median H3K27ac score  
219 in neuroblastoma cell line groups I and II, respectively. TFs are indicated in black with arrows.  
220 **d, e,** Tracks for ChIP-seq profiles for H3K27ac binding at *ALK* and *PHOX2B* SEs, respectively.  
221 **f,** Western blot analysis of PHOX2B and vinculin as a loading control in a panel of  
222 neuroblastoma cell lines. *SK-N-SH cells correspond to batch 1.* **g,** TFs predicted to participate in  
223 a CRC with PHOX2B (upper part) or with a FOS/JUN family member (lower part) in  
224 neuroblastoma cell lines. TFs whose binding motifs are enriched in SEs of group I and II are  
225 shown in bold. **h,** Pearson correlation matrix for the *expression values of 22 TFs identified in*  
226 *CRCs of cell lines shows strong positive correlations within module 1 and module 2; correlation*  
227 *is calculated for RNA-seq data in neuroblastoma cell lines and PDX (n=31).* **i,** Single cell  
228 analysis reveals heterogeneity of cell identity in the SK-N-AS cell line. Expression of TF of  
229 modules 1 and 2 was evaluated by RT-q-PCR and data were normalized to the SK-N-AS cell  
230 population overall.

231  
232  
233  
234  
235  
236



237

238 **Figure 2. Different identity of neuroblastoma primary tumors and impact of chemotherapy**

239 **on cell identity.** **a**, Pearson correlation matrix for the 22 TFs identified in CRCs of cell lines in a

240 set of 498 neuroblastoma primary tumors. **b**, Mean expressions of the noradrenergic and NCC-

241 like modules negatively correlate in the whole set of tumors (Pearson  $R = -0.49$ , one-sided

242 permutation test  $p\text{-value} < 10^{-10}$ ) and define a continuum between full noradrenergic and NCC-

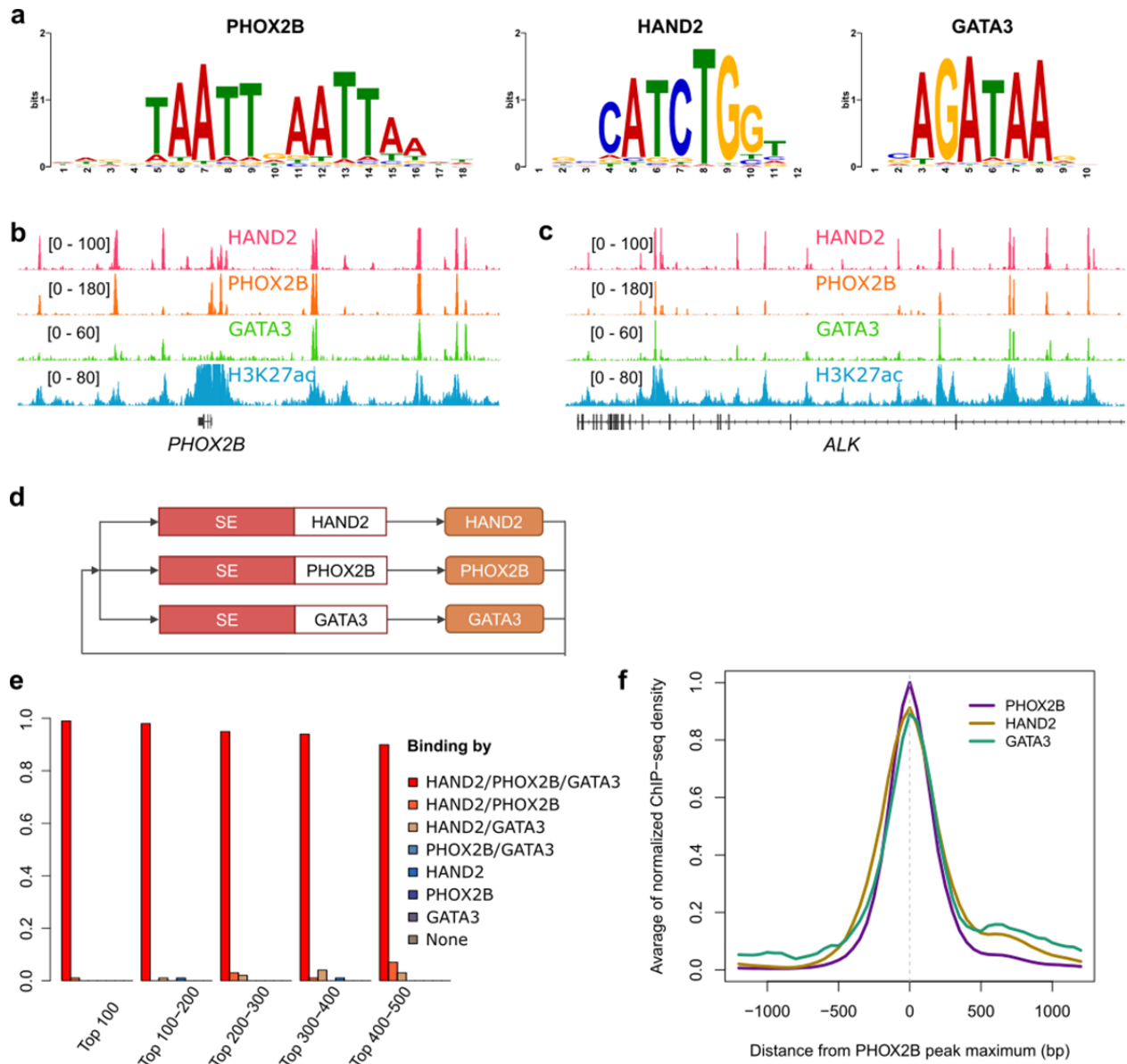
243 like cases. Blue: tumors with *MYCN* amplification. **c**, Identity of tumor pairs at diagnosis and

244 relapse revealed by expression profiling. The series includes 7 pairs from the GSE65303

245 dataset<sup>22</sup> (red) and 3 in-house pairs (black). **d**, Treatment of SK-N-SH cells with chemotherapy

246 favors cells with an NCC-like identity. Cells used in this experiment (batch 2) were more

247 noradrenergic compared to the ones used in the ChIP-seq experiment (batch 1).



248

249 **Figure 3. PHOX2B, HAND2 and GATA3 are master transcription factors defining the SE**

250 **landscape of noradrenergic neuroblastoma. a, De novo** identification of PHOX2B, HAND2

251 and GATA3 TF binding motifs. **b and c,** Tracks for CHIP-seq profiles for PHOX2B, HAND2,

252 GATA3 and H3K27ac binding at *PHOX2B* and *ALK* SEs, respectively. **d,** CRC of activating TFs

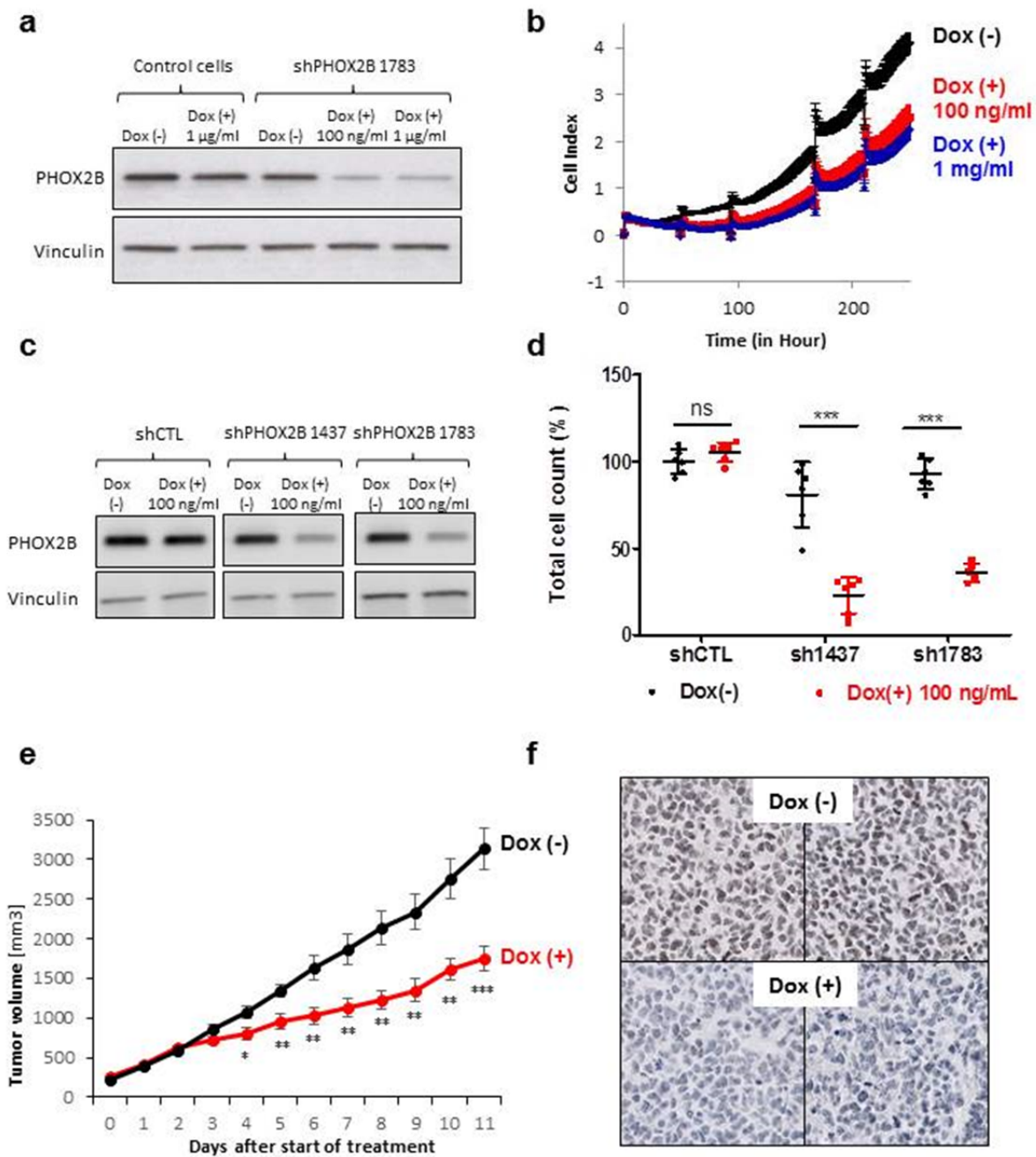
253 that define a noradrenergic module. **e,** Neuroblastoma SEs defined by H3K27ac peaks are

254 **simultaneously** occupied by PHOX2B, HAND2 and GATA3. **f,** HAND2, PHOX2B and GATA3

255 bind closely located regions within neuroblastoma SEs (summary of densities of 2,078 binding

256 sites corresponding to 500 top neuroblastoma SEs).

257



258

259

260 **Figure 4. PHOX2B is critical for the growth of noradrenergic neuroblastoma cells. a,**  
 261 **PHOX2B knockdown following doxycycline treatment was confirmed at 72 h by immunoblot**  
 262 **(loading control: vinculin) in CLB-GA neuroblastoma cells infected with a shRNA targeting**  
 263 **PHOX2B vector. b, xCELLigence™ proliferation kinetics of infected CLB-GA cells in absence**

264 or presence of doxycycline at 100 ng/ml or 1  $\mu$ g/ml. Data shown are the mean  $\pm$  s.d. of results  
265 obtained in the different conditions (n=5 technical replicates). **c**, PHOX2B immunoblot of SH-  
266 SY5Y neuroblastoma cells infected with 2 different shRNA vectors targeting *PHOX2B*, at 72 h.  
267 **d**, Cell counts for the SH-SY5Y cell line infected with sh1437 or sh1783 vectors targeting  
268 PHOX2B or with the control shCTL vector.  $10^5$  cells were plated in 24-well plates at day 0 in the  
269 absence or presence of doxycycline at 100 ng/ml. The number of living cells was counted at day  
270 8 (Mean  $\pm$  s.d.; n=6 replicates). **e**, Growth curves for subcutaneously xenografted sh1783  
271 transduced CLB-GA cells. When tumors reached a volume of around 170 mm<sup>3</sup>, doxycycline and  
272 sucrose (Dox +) or sucrose alone (Dox -) was added to the drinking water (Mean  $\pm$  s.e.m.; n =8  
273 mice per group). P values were determined via two-tailed unpaired Welch's t-test (\*\*\*:  
274 p<0.001). **f**, PHOX2B immunohistochemistry (brown) combined with Hematoxylin staining in  
275 two xenografts treated with doxycycline and two control xenografts.

276

277

278

279

280

281

282

283

284

285

286

287

288 **References**

- 289 1. Matthay, K. K. *et al.* Neuroblastoma. *Nat. Rev. Dis. Primer* **2**, 16078 (2016).
- 290 2. Brodeur, G. M., Seeger, R. C., Schwab, M., Varmus, H. E. & Bishop, J. M. Amplification  
291 of N-myc in untreated human neuroblastomas correlates with advanced disease stage. *Science*  
292 **224**, 1121–4 (1984).
- 293 3. Mosse, Y. P. *et al.* Identification of ALK as a major familial neuroblastoma  
294 predisposition gene. *Nature* **455**, 930–5 (2008).
- 295 4. Janoueix-Lerosey, I. *et al.* Somatic and germline activating mutations of the ALK kinase  
296 receptor in neuroblastoma. *Nature* **455**, 967–70 (2008).
- 297 5. George, R. E. *et al.* Activating mutations in ALK provide a therapeutic target in  
298 neuroblastoma. *Nature* **455**, 975–8 (2008).
- 299 6. Chen, Y. *et al.* Oncogenic mutations of ALK kinase in neuroblastoma. *Nature* **455**, 971–4  
300 (2008).
- 301 7. Peifer, M. *et al.* Telomerase activation by genomic rearrangements in high-risk  
302 neuroblastoma. *Nature* **526**, 700–704 (2015).
- 303 8. Valentijn, L. J. *et al.* TERT rearrangements are frequent in neuroblastoma and identify  
304 aggressive tumors. *Nat. Genet.* **47**, 1411–1414 (2015).
- 305 9. Saint-André, V. *et al.* Models of human core transcriptional regulatory circuitries.  
306 *Genome Res.* **26**, 385–396 (2016).
- 307 10. Hnisz, D. *et al.* Super-enhancers in the control of cell identity and disease. *Cell* **155**, 934–  
308 947 (2013).
- 309 11. Thomas, S. *et al.* Human neural crest cells display molecular and phenotypic hallmarks of  
310 stem cells. *Hum Mol Genet* **17**, 3411–25 (2008).
- 311 12. Whyte, W. A. *et al.* Master transcription factors and mediator establish super-enhancers  
312 at key cell identity genes. *Cell* **153**, 307–319 (2013).
- 313 13. Ross, R. A., Spengler, B. A. & Biedler, J. L. Coordinate morphological and biochemical  
314 interconversion of human neuroblastoma cells. *J. Natl. Cancer Inst.* **71**, 741–747 (1983).
- 315 14. Chipumuro, E. *et al.* CDK7 Inhibition Suppresses Super-Enhancer-Linked Oncogenic  
316 Transcription in MYCN-Driven Cancer. *Cell* **159**, 1126–1139 (2014).
- 317 15. Oldridge, D. A. *et al.* Genetic predisposition to neuroblastoma mediated by a LMO1  
318 super-enhancer polymorphism. *Nature* **528**, 418–421 (2015).

- 319 16. Rohrer, H. Transcriptional control of differentiation and neurogenesis in autonomic  
320 ganglia. *Eur J Neurosci* **34**, 1563–73 (2011).
- 321 17. Pattyn, A., Morin, X., Cremer, H., Goridis, C. & Brunet, J. F. The homeobox gene  
322 Phox2b is essential for the development of autonomic neural crest derivatives. *Nature* **399**, 366–  
323 70 (1999).
- 324 18. Flora, A. *et al.* Sp proteins and Phox2b regulate the expression of the human Phox2a  
325 gene. *J. Neurosci.* **21**, 7037–7045 (2001).
- 326 19. Lin, C. Y. *et al.* Active medulloblastoma enhancers reveal subgroup-specific cellular  
327 origins. *Nature* **530**, 57–62 (2016).
- 328 20. Zhang, W. *et al.* Comparison of RNA-seq and microarray-based models for clinical  
329 endpoint prediction. *Genome Biol.* **16**, (2015).
- 330 21. Wakamatsu, Y., Watanabe, Y., Nakamura, H. & Kondoh, H. Regulation of the neural  
331 crest cell fate by N-myc: promotion of ventral migration and neuronal differentiation.  
332 *Development* **124**, 1953–62 (1997).
- 333 22. Schramm, A. *et al.* Mutational dynamics between primary and relapse neuroblastomas.  
334 *Nat. Genet.* **47**, 872–877 (2015).
- 335 23. Reiff, T. *et al.* Neuroblastoma phox2b variants stimulate proliferation and  
336 dedifferentiation of immature sympathetic neurons. *J. Neurosci.* **30**, 905–915 (2010).
- 337 24. Chapuy, B. *et al.* Discovery and characterization of super-enhancer-associated  
338 dependencies in diffuse large B cell lymphoma. *Cancer Cell* **24**, 777–790 (2013).
- 339 25. Trochet, D. *et al.* Germline mutations of the paired-like homeobox 2B (PHOX2B) gene  
340 in neuroblastoma. *Am J Hum Genet* **74**, 761–4 (2004).
- 341 26. Mosse, Y. P. *et al.* Germline PHOX2B mutation in hereditary neuroblastoma. *Am J Hum*  
342 *Genet* **75**, 727–30 (2004).
- 343 27. Coppola, E., d’Autréaux, F., Rijli, F. M. & Brunet, J.-F. Ongoing roles of Phox2  
344 homeodomain transcription factors during neuronal differentiation. *Development* **137**, 4211–  
345 4220 (2010).
- 346 28. Ke, X.-X. *et al.* Phox2B correlates with MYCN and is a prognostic marker for  
347 neuroblastoma development. *Oncol. Lett.* **9**, 2507–2514 (2015).
- 348 29. Garraway, L. A. & Sellers, W. R. Lineage dependency and lineage-survival oncogenes in  
349 human cancer. *Nat. Rev. Cancer* **6**, 593–602 (2006).



## 350 **Online Methods**

351

### 352 **Neuroblastoma and hNCC cell lines**

353

354 Neuroblastoma cell lines used in this study have been previously described<sup>30</sup>. **CHP-212, IMR-32,**  
355 **SH-SY5Y, SK-N-AS, SK-N-BE(2)C, SK-N-DZ, SK-NF-I and SK-N-SH** were obtained from the  
356 American Type Culture Collection (ATCC). CLB cell lines were derived by V. Combaret (Lyon,  
357 France). The SH-EP and LAN-1 cell lines have been kindly provided by M. Schwab  
358 (Heidelberg, Germany) and J. Couturier (Paris, France). Lines GIMEN, N206, SJNB1, SJNB6,  
359 SJNB8, SJNB12 and TR-14 were obtained from R. Versteeg (Amsterdam, The Netherlands) and  
360 line GICAN was a kind gift from M. Ponzoni (Genova, Italy). The NB69 and NB-EBc1 cell lines  
361 were obtained from the European Collection of Authenticated Cell Cultures and from the  
362 Children's Oncology Group, respectively. A first batch of SK-N-SH cells (batch 1) was used for  
363 the ChIP-seq and single cell analysis. A second batch (batch 2) was used for the evaluation of the  
364 chemotherapeutic agents. Batch 2 was enriched in adrenergic cells. Cell line authentication was  
365 performed by comparison of the genomic copy number profile calculated from the input ChIP-  
366 seq data obtained using Control-FREEC<sup>31</sup> (see below) with SNP array profile and STR profiling  
367 for ATCC cell lines. Cells were checked routinely by PCR for the absence of mycoplasma.  
368 Neuroblastoma cell lines were cultured at 37°C with 5% CO<sub>2</sub> in a humidified atmosphere in  
369 RPMI (GE Healthcare, for CLB cell lines, SH-EP, GICAN and NB69), in IMDM (Gibco) for  
370 NB-EBc1 (according to the provided conditions) or DMEM (GE Healthcare, for other cell lines),  
371 with 10%, 15% or 20% FCS (Eurobio) and 100 µg/ml penicillin/streptomycin (Gibco). Primary  
372 hNCC lines were grown as previously described<sup>32</sup> under bioethical approval PFS14-011 from the  
373 French Biomedical Agency for the use of human embryonic material to S. Zaffran. Briefly, cells  
374 were grown in Glutamax DMEM:F12 [Gibco] supplemented with 12% FCS (Eurobio), 100  
375 µg/ml penicillin/streptomycin, 10 mM HEPES, 100 ng/ml hydrocortisone, 10 µg/ml transferrin,  
376 400 pg/ml 3,3,5-thio-iodo-thyronine, 10 pg/ml glucagon, 100 pg/ml epidermal growth factor, 1  
377 ng/ml insulin and 200 pg/ml fibroblast growth factor 2 (all products supplied by Sigma-Aldrich  
378 except EGF and FGF2 from Gibco).

379

380

381 **PDX models**

382

383 Neuroblastoma PDXs were obtained from stage L2 (MAP-IC-A23-NB-1), stage 3 (IGR-NB8) or  
384 stage 4 (IGR-N835, MAP-GR-A99-NB-1, MAP-GR-B25-NB-1 and HSJD-NB-011<sup>33</sup>). None of  
385 them was related to the used cell lines. All PDXs but MAP-IC-A23-NB-1 had *MYCN*  
386 amplification. PDXs IGR-NB8, IGR-N835<sup>34,35</sup> were obtained using female Swiss nude mice of  
387 6-8 weeks at engraftment whereas female NSG mice were used for MAP-GR-A99-NB-1 and  
388 MAP-GR-B25 PDXs. These PDX models are developed and maintained within the project  
389 "Development of Pediatric PDX models" approved by the experimental ethic committee 26  
390 (CEEA26 – Gustave Roussy) under the number 2015032614359689v7. The MAP-IC-A23-NB-1  
391 (IC-pPDX-17) and HSJD-NB-011 models were obtained using female SCID mice of 10-11  
392 weeks or female Swiss nude mice of 3-6 weeks at engraftment. Animal studies at SJD were  
393 approved by the local animal care and use committee (Comite Etico de Experimentacion Animal  
394 at Universidad de Barcelona, protocol 135/11). All experiments were performed in accordance  
395 with European legislation. MAP-IC-A23-NB-1, MAP-GR-A99-NB-1 and MAP-GR-B25-NB-1  
396 PDXs were obtained through the Mappyacts protocol (clinicaltrial.gov: NCT02613962).

397

398 **Patient samples**

399

400 Three diagnosis/relapse pairs of tumors (Pair1/2/3-Diagnosis and Relapse; all stage 4; Table S2)  
401 were studied in this work. The relapse samples were obtained through the Mappyacts protocol.  
402 The MAP-GR-B25-NB-1 PDX was derived from the relapse of pair 1. Analysis of biological  
403 material from patients, including study of expression profiles of neuroblastoma samples was  
404 approved by the Institut Curie's Institutional Review Board. This study was authorized by the  
405 decision of the ethics committees « Comité de Protection des Personnes Sud-Est IV », references  
406 L07–95 and L12–171, “Comité de Protection des Personnes Ile de France 1”, reference 0811728  
407 and “Comité de Protection des Personnes Ile de France 3” reference 3272. Written informed  
408 consent was obtained from parents or guardians according to national law.

409

410

411

## 412 **ChIP-sequencing**

413

414 H3K27ac, PHOX2B, HAND2 and GATA3 chromatin immunoprecipitation (ChIP) was  
415 performed using the iDeal ChIP-seq kit for Histones or iDeal ChIP-seq kit for Transcription  
416 Factors (Diagenode) using the following antibodies: ab4729 (rabbit polyclonal, Abcam) for  
417 H3K27ac, sc-376997X (mouse monoclonal), sc-9409 and sc-22206X (goat polyclonal) from  
418 Santa Cruz Biotechnology for PHOX2B, HAND2 and GATA3, respectively. Ten million cells  
419 were cross-linked with 1% formaldehyde for 10 min followed by quenching with 125 mM  
420 glycine final concentration for 5 min at room temperature. Chromatin was isolated by the  
421 addition of lysis buffer, and lysates sonicated to obtain sheared chromatin to an average length of  
422 ~ 300 bp. ChIP was performed with chromatin of 1 million cells for H3K27ac and 3.75 million  
423 cells for transcription factors. The equivalent of 1% of chromatin **used for TFs** was kept to  
424 quantify input and reverse cross-linked 4h at 65°C with proteinase K. ChIP was performed  
425 overnight at 4°C on a rotating wheel with 1 µg of antibody for H3K27ac, 2 µg for HAND2 and 5  
426 µg for PHOX2B and GATA3. Protein A-coated magnetic beads were precleared with antibodies  
427 3h at 4°C only for transcription factors. After ChIP, chromatin was eluted 30 min at room  
428 temperature and reverse cross-linked 4h at 65°C with proteinase K. DNA was precipitated and  
429 purified with magnetic beads with the Ipure kit (Diagenode). Before sequencing, ChIP efficiency  
430 was validated by quantitative PCR for each antibody on specific genomic regions using  
431 powerSYBR® Green Master mix (Applied Biosystems) and compared for each primer pair to the  
432 input DNA. Primers are available upon request.

433 For PDX samples, frozen tumors were reduced to powder with a pestle and then resuspended in  
434 PBS. Crosslinking of chromatin was performed by adding 1% formaldehyde for 8 min with  
435 agitation on a rotating wheel. Lysis of cells, fragmentation of chromatin and ChIP were  
436 performed as described above for cell lines using the iDeal ChIP-seq kit for Histones.

437 Illumina sequencing libraries were prepared from ChIP and input DNA using the TruSeq ChIP  
438 library preparation kit according to the manufacturer's protocol. Briefly, DNA were subjected to  
439 consecutive steps of end-repair, dA-tailing and ligation to TruSeq indexed Illumina adapters.  
440 Size-selection was performed only for the H3K27ac ChIP (100 – 600 bp). After a final  
441 amplification step **of 14 cycles**, the resulting DNA libraries were quantified using a qPCR  
442 method (KAPA library quantification kit) and sequenced on the Illumina HiSeq2500 instrument

443 (rapid run mode; single reads 100 nts).

444

#### 445 **ChIP-seq analysis**

446

447 ChIP-seq reads were mapped to the human reference genome hg19/GRCh37 using Bowtie2  
448 v2.1.0<sup>36</sup>. Low mapping quality reads (Q<20) were discarded; duplicate reads were kept in order  
449 to detect signal in genomic amplification regions. Enriched regions (peaks) were called using  
450 HMCAN v1.30<sup>37</sup> with the following parameters: min fragment length 100 bp, median fragment  
451 length 250 bp, maximal fragment length 400 bp, small bin length 50 bp, large bin length 25 kb,  
452 p-value threshold 0.05, merging distance 200 bp, number of iterations 20, final threshold 0.1,  
453 removing duplicates: False. Regions from the hg19 ENCODE blacklist<sup>38</sup> were excluded from the  
454 analysis. HMCAN output included ChIP density profiles corrected for the GC-content and copy  
455 number bias (\*.wig) and narrow and large enrichment regions further called peaks (\*.bed).  
456 Density profiles were then normalized between samples with an in-house R script based on the  
457 median density values in the 5,000 highest peaks discounting the first 100 peaks as they may  
458 correspond to amplification regions. Peaks with low signal (i.e., low HMCAN score values) were  
459 discarded (in-house script correlating peak length and peak signal,  
460 <https://github.com/BoevaLab/LILY/>).

461 The Control-FREEC<sup>31</sup> algorithm was applied to input samples (default parameters; input: \*.bam  
462 files) to obtain copy number profiles of each cell line. These profiles matched known copy  
463 number profiles for these neuroblastoma cell lines.

464 To call enhancers and super-enhancers, a modified version of ROSE<sup>12,39</sup> dubbed LILY was used  
465 (<http://BoevaLab.com/LILY/>). First, large H3K27ac peaks were stitched together, using a default  
466 distance of 12.5 kb, while promoter regions ( $\pm$  2.5 Kb from the transcription start site) were  
467 excluded. Then each region received a SE score corresponding to the sum of normalized  
468 H3K27ac density values (already corrected for copy number and GC-content bias by HMCAN<sup>37</sup>).  
469 The regions were sorted according to the SE score. The threshold of the score distinguishing  
470 typical enhancers from SEs was determined by ROSE. For twenty-five neuroblastoma cell lines,  
471 the average number of SEs identified per cell line was 1,252 (standard deviation 385). The  
472 highest number of SEs was detected in GIMEN and SH-EP (1,901 and 1,819 regions  
473 respectively).

474 ChIP-seq experiments for H3K27ac were performed once for every sample except for the CLB-  
475 GA cell line for which the experiment was performed in two biological replicates. We used these  
476 replicate samples to document the reproducibility of the SE calling and SE score calculation  
477 (Figure S21). Among the top 500 SEs of replicate 1, 93% were annotated as active SEs in  
478 replicate 2.

479 To generate a list of neuroblastoma SEs, we superimposed the SE regions predicted in the  
480 twenty-five cell lines and excluded regions shorter than 12 Kb. In order to avoid stitching of  
481 several neighboring SE regions into one, long regions with several sub-peaks were separated in  
482 sub-regions using as a threshold one half of the median number of SEs. Overall, 4,336 regions  
483 with overlapping SEs detected in more than one sample were annotated as putative  
484 neuroblastoma SEs (Table S3). SEs were assigned to the RefSeq genes (hg19, version Sep 16,  
485 2016) using the information about locations of topologically associating domains (TADs) in  
486 eight human cell lines<sup>40</sup>. Among all genes located in the same TAD with a SE and therefore  
487 possibly regulated by a SE, we selected these with the highest correlation between the gene  
488 expression and the SE score in the 33 samples of these study (threshold 0.361 corresponding to  
489 the adjusted p-value ('FDR') of 0.05, Figure S11). Of note, each gene can have several SE  
490 regions and each SE can be assigned to a number of genes (Table S3). In total, neuroblastoma  
491 SEs were assigned to 4,791 genes. Similarly, we detected and assigned to genes 1,639 SEs active  
492 in both hNCC samples.

493 For further analysis, we kept only SE regions active in at least two neuroblastoma cell lines or  
494 hNCC samples (5,975 regions). This was done to remove cell-line specific events and false  
495 positive predictions of SE regions.

496 Principal Component Analysis (PCA) for 33 samples (25 neuroblastoma cell lines, 6  
497 neuroblastoma PDXs and 2 hNCC lines) was performed on log<sub>2</sub> values of SE scores of 5,975  
498 SEs. Table S3 shows contributions of the SE regions to the first two principal components.  
499 Analysis of samples in the first principal components suggested their separation into group I  
500 (CLB-GA, CLB-MA, CLB-CAR, CLB-BER-Lud, CLB-PE, NB69, NB-EBc1, SJNB1, SJNB6,  
501 SJNB8, IMR-32, LAN-1, N206, SK-N-BE(2)C, SK-N-DZ, SK-N-FI, TR14, SH-SY5Y), group II  
502 (GICAN, SH-EP, GIMEN) and the intermediate group (SK-N-SH, SK-N-AS, SJNB12, CHP-  
503 212). Table S3 includes information about fold changes and p-values for the two-sided Wilcoxon  
504 test for differential analysis of SE scores between group I and II.

505 To detect known transcription factor binding motifs enriched in neuroblastoma SEs (cell lines of  
506 group I and II) and SEs of hNCC, we applied the i-cisTarget<sup>41</sup> method to the list of 2,227, 1,850  
507 and 1,640 valley regions in H3K27ac peaks overlapping the 100 top SEs of group I and II and  
508 hNCC, respectively.

509 CRC in the neuroblastoma cell lines, PDX samples and hNCC lines were detected using  
510 COLTRON<sup>19</sup> based on the list of samples' SEs with the following properties: (i) SE score  
511 correlated with gene expression in our set of 31 NB samples and (2) SE region was detected in  
512 more than 2 cell lines in our study. We then parsed the files with ranked cliques to see whether a  
513 given TF was predicted to be involved in a CRC of a given sample. We kept TFs present in over  
514 50% of cell lines from group I (n=18) or group II (n=3). This resulted in 69 TFs. From the  
515 COLTRON predictions, we excluded 17 transcription factors that were not associated with a SE  
516 in our analysis (Figure S10). As motif enrichment analysis discovered a significant enrichment in  
517 homeobox and AP-1 motifs of neuroblastoma SEs (Figures S4 and S8), among these 52 TFs, we  
518 selected those that were predicted by COLTRON to occur in the same CRC as the homeobox TF  
519 PHOX2B or AP-1 TFs (JUN, JUNB, FOSL1 or FOSL2) in more than 50% of cell lines of group  
520 I or II. This resulted in 37 TFs (Figure 1g). Clustering of the 37 genes (hclust, McQuitty method)  
521 based on the correlation of their expression defined two modules (module 1, n = 7, includes  
522 PHOX2B; module 2, n=15, includes FOSL1 and FOSL2) (Figure S22).

523 Motif discovery in ChIP-seq peaks of GATA3, HAND2 and PHOX2B was performed using the  
524 Position Analysis tool of the RSAT package<sup>42</sup> (Oligonucleotide size: HAND2: 5; GATA3: 5;  
525 PHOX2B: 8).

526 To calculate average ChIP-seq density profiles around the PHOX2B peak maximum positions,  
527 we first extracted all 2,400 bp regions centered on PHOX2B ChIP-seq binding sites and kept  
528 those that overlapped peaks of all three TFs. We obtained 14,693 such regions throughout the  
529 whole human genome for the CLB-GA cell line. 2,078 out of them were located within the 500  
530 strongest neuroblastoma SEs. ChIP-seq density for each TF for each region was rescaled to have  
531 a maximum value of 1 corresponding to the peak maximum. We then plotted the average  
532 rescaled density for the 2,078 regions.

533

### 534 **RNA-sequencing and transcriptome read alignment**

535 Total RNA was extracted from fresh cells or frozen tumors using TRIzol® Reagent (Invitrogen),

536 or AllPrep DNA/RNA Mini Kit (Qiagen) or NucleoSpin RNA kit (Macherey-Nagel; for the SK-  
537 N-SH cell line treated with chemotherapy). All samples were subjected to quality control on a  
538 Bioanalyzer instrument and only RNA with RIN (RNA Integrity Number) > 6 were used for  
539 sequencing. RNA sequencing libraries were prepared from 1 µg of total RNA using the Illumina  
540 TruSeq Stranded mRNA Library preparation kit which allows performing a strand-specific  
541 sequencing. A first step of polyA selection using magnetic beads is done to focus sequencing on  
542 polyadenylated transcripts. After fragmentation, cDNA synthesis was performed and resulting  
543 fragments were used for dA-tailing and then ligated to the TruSeq indexed adapters. PCR  
544 amplification is finally achieved to create the final cDNA library. After qPCR quantification,  
545 sequencing was carried out using 2 x 50 cycles (paired-end reads 50 nts) for all samples (except  
546 SH-EP, 2 x 100; Pair1-Relapse and Pair3-Relapse, 2 x 75; Pair2-Relapse, 2 x 150). Sequencing  
547 was performed with the Illumina HiSeq2500 instrument (high output mode) except for cases  
548 Pair1-Relapse and Pair2-Relapse analyzed with the NextSeq500 instrument and Pair3-Relapse3  
549 analyzed on a HiSeq4000 instrument. Reads were aligned to the human reference genome  
550 hg19/GRCh37 using TopHat2 v2.0.6<sup>43</sup> with the following parameters: global alignment, no  
551 mismatch in the 22 bp seed, up to three mismatches in the read, library type fr-firststrand.  
552 Gene expression values (FPKM=fragments per kilobase per million reads) were computed by  
553 Cufflinks v2.2.1<sup>44</sup> and further normalization between samples was done using quantile  
554 normalization (R/Bioconductor package limma)<sup>45</sup>.

555

## 556 **Western blots**

557

558 Western blots were carried out using standard protocols with the following antibodies: PHOX2B  
559 (sc-376997 from Santa Cruz Biotechnology at 1:500) and anti-vinculin (ab18058 from Abcam at  
560 1:1,000). Membranes were then incubated with an anti-mouse immunoglobulin G (IgG)  
561 horseradish peroxidase–coupled secondary antibody (1:3,000, NA931V) from GE Healthcare.  
562 Proteins were detected by enhanced chemiluminescence (PerkinElmer).

563

## 564 **Single cell gene expression analysis**

565 Single cells loading, capture and mRNA pre-amplification were performed following the  
566 Fluidigm user manual “Using C1 to Capture Cells from Cell Culture and Perform

567 Preamplification Using Delta Gene Assays". Briefly, cells were dissociated using TrypLE  
568 Express reagent (Gibco), washed 2 times in PBS and 2,000-4,000 cells were loaded onto a  
569 medium size (10-17µm) C1 single-cell auto prep IFC (Fluidigm). The capture efficiency was  
570 assessed by imaging capture sites under the microscope and cell viability was investigated with  
571 ethidium homodimer-1 and calcein AM stains (LIVE/DEAD kit, Thermo Fisher Scientific).  
572 Capture sites containing more than one cell or a dead cell were later excluded. Lysis, reverse  
573 transcription, and specific target preamplification steps were done on the C1 machine according  
574 to the Fluidigm user manual. Preamplification was done with inventoried pairs of unlabeled  
575 primers coupled with a Taqman probe FAM-MGB (Applied Biosystems TaqMan Gene  
576 Expression Assays, Thermo Fischer Scientific) for each of the module 1 and 2 genes and 4  
577 housekeeping genes (GAPDH, ACTG1, ACTB and RPL15). Preamplification products were  
578 harvested and high throughput real-time PCR was performed using the Fluidigm Biomark HD  
579 system with 48.48 gene expression Dynamic Arrays. For each cell line, a bulk control  
580 representative of 400 cells was processed the same way as the single cells. The raw data were  
581 first analyzed with the Fluidigm Real-Time PCR Analysis Software and exported to csv files for  
582 further analysis.

583 Gene expression value was normalized using the geometric mean of all 4 housekeeping genes Ct  
584 values of a given cell, cells were excluded if this geometric mean was >16.5. The Livak method  
585 ( $2^{-\Delta\Delta C_t}$ ) was applied using the gene expression values of the SK-N-SH cell line population as  
586 reference for the relative expression. Hierarchical clustering was performed using one minus  
587 Pearson correlation with an average linkage method including heatmap using Morpheus platform  
588 (<https://software.broadinstitute.org/morpheus>).

589

### 590 **Treatment of cell lines with chemotherapy**

591 SH-EP and SH-SY5Y cell lines were plated in 96-well plates two days before the addition of  
592 cisplatin, etoposide or doxorubicin. Seeding densities for each cell lines were optimized to reach  
593 80% of confluency in the untreated cells. Cells were treated with chemotherapeutic agents for 48  
594 h. Cell viability was then measured using the *in vitro* Toxicology Assay Kit, Resazurin-based,  
595 following manufacturer's instructions (Sigma-Aldrich).

596 SK-N-SH cells were plated in 6-well plates and then treated with cisplatin (7.5 µM) or



597 doxorubicin (100 nM) for 7 days, medium and drugs were changed every 2 days. RNAs were  
598 extracted using NucleoSpin RNA kit (Macherey-Nagel).

### 599 **Doxycycline-inducible shRNA systems**

600 PHOX2B-specific short hairpin RNAs sh1783 (5'-CCGGTGGAAGGCAGAAACCATTAAA-  
601 CTCGAGTTTAATGGTTTCTGCCTTCCATTTTGTG-3') and sh1437 (5'-CCGGAGTAATCG-  
602 CGCTAAGAATAAACTCGAGTTTATTCTTAGCGCGATTACTTTTTTTG-3') were selected  
603 from Sigma Mission shRNA library and cloned into the pLKO-Tet-On all-in-one system<sup>46</sup>  
604 (Addgene). Lentiviral particles were produced in HEK293T cells and CLB-GA cells were  
605 infected as previously described<sup>4</sup>. SH-SY5Y cells were incubated with viral particles for 48  
606 hours without polybrene. Selection with puromycin (Invitrogen) at 400 ng/ml or 1 µg/ml,  
607 respectively, was performed 24 h after infection and maintained during all culture experiments,  
608 for CLB-GA and SH-SY5Y cells, respectively. PHOX2B knockdown efficacy was assessed by  
609 Western blot 24 h/48 h/96 h after the addition of doxycycline (100 ng/ml or 1 µg/ml). For colony  
610 formation assays,  $6 \times 10^4$  transduced cells were plated at day 0 in 6-well dishes and stained with  
611 crystal violet at day 11<sup>47</sup>.

### 612 **Proliferation assays**

613 Cells were counted in real-time with an xCELLigence<sup>TM</sup> instrument (ACEA Biosciences)  
614 monitoring impedance across gold microelectrodes.  $10^4$  infected CLB-GA or SH-SY5Y cells  
615 were seeded per well of a 96-well plate in 200 µl medium containing doxycycline at 100 ng/ml  
616 or 1 µg/ml (quintuplicates per group) or no doxycycline. Medium was refreshed after 48 h. For  
617 cell counting,  $2 \times 10^4$  infected CLB-GA or  $10^5$  infected SH-SY5Y were plated in 24-well plates in  
618 the presence or absence of doxycycline at 100 ng/ml or 1 µg/ml. The number of living cells was  
619 counted at day 4, 7, 10 and 14 (triplicates per group) for CLB-GA and at day 8 (n=5/6 technical  
620 replicates) for SH-SY5Y cells using a Vi-cell XR Cell Viability Analyzer (Beckman Coulter)

621

622

### 623 **Statistical analysis**

624 To calculate p-values for Pearson correlation (null hypothesis consisted in zero Pearson  
625 correlation), we implemented a one-sided permutation test. Number of permutations was  $10^4$

626 when calculating p-values for correlation between SE score and gene expression (Figure S11)  
627 and  $10^6$  in the test for correlation between gene expression of the noradrenergic and NCC-like  
628 modules in the set of tumors (Figure 2). This test does not need the data to follow the normal  
629 distribution and does not require equal variation between the groups that are statistically  
630 compared.

631

### 632 **Xenotransplantation experiments and mice**

633  $10 \times 10^6$  CLB-GA cells transduced with the shRNA against PHOX2B (sh1783) were injected  
634 subcutaneously in the flanks of 6-week-old NSG mice (Charles Rivers Laboratories) in an equal  
635 mix of PBS and Matrigel (BD Biosciences). When tumors reached a volume of around  $170 \text{ mm}^3$ ,  
636 mice were randomly assigned to the control (5% sucrose in drinking water) or the treatment  
637 (doxycycline (2 mg/l) and 5% sucrose in drinking water) groups. Tumor growth was monitored  
638 with a caliper every day. Mice were killed once tumors reached a volume of around  $3,000 \text{ mm}^3$   
639 calculated as  $V = a/2 \times b \times ((a+b)/2)$  with a being the largest diameter and b the smallest.  
640 Experiments were conducted in accordance with the recommendations of the European  
641 Community (86/609/EEC), the French Competent Authority, and UKCCCR (guidelines for the  
642 welfare and use of animals in cancer research). Approval for this study was received from  
643 Ministère de l'Education Nationale, de l'Enseignement Supérieur et de la Recherche  
644 (authorization number 5524-20 160531 1607151 v5).

645

### 646 **PHOX2B immunohistochemistry**

647 Mice tumors were fixed with acidified formal alcohol (AFA) for 24 h and paraffin-embedded.  
648 Labelling was performed on  $4 \mu\text{m}$  sections with the BOND-III instrument (Leica Microsystems)  
649 using the Bond Polymer Refine Detection™ (Leica) kit. Briefly, sections were deparaffinized,  
650 antigen retrieval was performed with an EDTA-based solution (Leica) for 20 minutes at pH 9,  
651 and sections were stained with a rabbit polyclonal anti-PHOX2B antibody (Abcam, EPR14423,  
652 1/1000).

653

### 654 **siRNA and growth assays**

655 HAND2 and GATA3 knockdown was performed with 20 nM siRNA (Hs\_HAND2\_3  
656 #SI00131915, Hs\_HAND2\_6 #SI03046736, Hs\_GATA3\_7 #SI04202681 and Hs\_GATA3\_8

657 #SI04212446; Control siRNA #1027281; Qiagen) using RNAimax transfection reagent (Thermo  
658 Fisher Scientific). The number of living cells was counted using a Vi-cell XR Cell Viability  
659 Analyzer (Beckman Coulter) (n=5 or 6 technical replicates).

660

#### 661 **Data Availability**

662 Raw data for cell line ChIP-seq and RNA-seq, and processed data for the cell lines, tumors and  
663 PDXs are available in Gene Expression Omnibus (GEO) under accession number GSE90683.

664 Raw data for PDX ChIP-seq and RNA-seq will be available through EGA, as well as RNA-seq  
665 data for patient samples.

666 Reviewers can access to the GEO submission using this link:

667 <https://www.ncbi.nlm.nih.gov/geo/query/acc.cgi?token=khcvkaailpulxqt&acc=GSE90683>.

#### 668 **Code availability**

669 The code of the pipeline for the SE detection from cancer ChIP-seq data is available at  
670 <http://boevalab.com/LILY/>.

671

672

673 30. Schleiermacher, G. *et al.* Combined 24-color karyotyping and comparative genomic  
674 hybridization analysis indicates predominant rearrangements of early replicating chromosome  
675 regions in neuroblastoma. *Cancer Genet Cytogenet* **141**, 32-42 (2003)

676 31. Boeva, V. *et al.* Control-free calling of copy number alterations in deep-sequencing data  
677 using GC-content normalization. *Bioinformatics* **27**, 268–9 (2011).

678 32. Etchevers, H. Primary culture of chick, mouse or human neural crest cells. *Nat. Protoc.* **6**,  
679 1568–1577 (2011).

680 33. Monterrubio, C. *et al.* Targeted drug distribution in tumor extracellular fluid of GD2-  
681 expressing neuroblastoma patient-derived xenografts using SN-38-loaded nanoparticles  
682 conjugated to the monoclonal antibody 3F8. *J. Control. Release* **255**, 108–119 (2017).

683 34. Vassal, G. *et al.* Therapeutic activity of CPT-11, a DNA-topoisomerase I inhibitor, against  
684 peripheral primitive neuroectodermal tumour and neuroblastoma xenografts. *Br. J. Cancer* **74**,  
685 537–545 (1996).

686 35. Bettan-Renaud, L., Bayle, C., Teyssier, J. R. & Benard, J. Stability of phenotypic and

687 genotypic traits during the establishment of a human neuroblastoma cell line, IGR-N-835. *Int. J.*  
688 *Cancer* **44**, 460–466 (1989).

689 36. Langmead, B. & Salzberg, S. L. Fast gapped-read alignment with Bowtie 2. *Nat. Methods* **9**,  
690 357–359 (2012).

691 37. Ashoor, H. *et al.* HMCan: a method for detecting chromatin modifications in cancer samples  
692 using ChIP-seq data. *Bioinformatics* **29**, 2979–2986 (2013).

693 38. ENCODE Project Consortium. An integrated encyclopedia of DNA elements in the human  
694 genome. *Nature* **489**, 57–74 (2012).

695 39. Lovén, J. *et al.* Selective inhibition of tumor oncogenes by disruption of super-enhancers.  
696 *Cell* **153**, 320–334 (2013).

697 40. Rao, S. S. P. *et al.* A 3D map of the human genome at kilobase resolution reveals principles  
698 of chromatin looping. *Cell* **159**, 1665–1680 (2014).

699 41. Herrmann, C., Van de Sande, B., Potier, D. & Aerts, S. i-cisTarget: an integrative genomics  
700 method for the prediction of regulatory features and cis-regulatory modules. *Nucleic Acids Res.*  
701 **40**, e114 (2012).

702 42. Medina-Rivera, A. *et al.* RSAT 2015: Regulatory Sequence Analysis Tools. *Nucleic Acids*  
703 *Res.* **43**, W50-56 (2015).

704 43. Kim, D. *et al.* TopHat2: accurate alignment of transcriptomes in the presence of insertions,  
705 deletions and gene fusions. *Genome Biol.* **14**, R36 (2013).

706 44. Trapnell, C. *et al.* Transcript assembly and quantification by RNA-Seq reveals unannotated  
707 transcripts and isoform switching during cell differentiation. *Nat. Biotechnol.* **28**, 511–515  
708 (2010).

709 45. Ritchie, M. E. *et al.* limma powers differential expression analyses for RNA-sequencing and  
710 microarray studies. *Nucleic Acids Res.* **43**, e47 (2015).

711 46. Wiederschain, D. *et al.* Single-vector inducible lentiviral RNAi system for oncology target  
712 validation. *Cell Cycle* **8**, 498–504 (2009).

713 47. Franken NAP, Rodermond HM, Stap J, Haveman J, van Bree C. Clonogenic assay of cells in  
714 vitro. *Nat Protoc.* 2006; 1:2315–2319.

715  
716  
717

718

719 **Acknowledgements**

720

721 This work was supported by grants from Institut Curie, Inserm, the Ligue Nationale Contre le  
722 Cancer (Equipe labellisée), the Société Française de Lutte contre les Cancers et les Leucémies de  
723 l'Enfant et l'Adolescent, the Institut National du Cancer (PRT-K14-061), the PHRC IC 2007-  
724 2009) and by the following associations: Association Hubert Guoin, Les Bagouz à Manon, les  
725 amis de Claire, Courir pour Mathieu, Dans les pas du Géant, Olivier Chape. The Mappyacts  
726 protocol is supported by the PRHC, the Fondation ARC, the Société Française de Lutte contre  
727 les Cancers et les Leucémies de l'Enfant et l'Adolescent (Fondation Enfants & Santé), the  
728 Fondation AREMIG and the Association Thibault BRIET). High-throughput sequencing has  
729 been performed by the ICGex NGS platform of the Institut Curie supported by the grants ANR-  
730 10-EQPX-03 (Equipex) and ANR-10-INBS-09-08 (France Génomique Consortium) from the  
731 Agence Nationale de la Recherche ("Investissements d'Avenir" program), by the Canceropole  
732 Ile-de-France and by the SiRIC-Curie program -SiRIC Grant "INCa-DGOS- 4654". Biomark  
733 analysis was done using the High Throughput qPCR-HD-Genomic Paris Centre platform  
734 supported by grants from "Région Ile-de-France". G.S. is supported by the Annenberg  
735 foundation. V.B. is supported by the ATIP-Avenir Program, the ARC Foundation (grant ARC -  
736 RAC16002KSA - R15093KS), Worldwide Cancer Research Foundation (grant WCR16-1294  
737 R16100KK) and the "Who Am I?" laboratory of excellence ANR-11-LABX-0071 funded by the  
738 French Government through its "Investissement d'Avenir" program operated by The French  
739 National Research Agency (ANR) (grant ANR-11-IDEX-0005-02). H.R. is supported by the  
740 Mayent-Rothschild program from Institut Curie and the Wilhelm-Sander-Stiftung. The  
741 laboratory of T.G.P.G. is supported by LMU Munich's Institutional Strategy LMUexcellent  
742 within the framework of the German Excellence Initiative, the 'Mehr LEBEN für krebskranke  
743 Kinder – Bettina-Bräu-Stiftung', the Walter Schulz Foundation, the Wilhelm-Sander-Stiftung  
744 (2016.167.1), and by the German Cancer Aid (DKH-111886 and DKH-70112257). We are  
745 grateful to M. Ponzoni (Genova, Italy) for providing the GICAN cell line, F. Tirode and C.  
746 Kamoun for help with RNA-seq analysis and alignment of NGS data, respectively, O. Blanchard  
747 for help in cell culture experiments and M. Caly for PHOX2B immunohistochemistry. We are  
748 grateful to the animal facilities team, the Experimental Pathology Department and the Plateforme

749 Génomique of Institut Curie. We thank N. Clément, T. Adam-de-Baumais and B. Mallon for  
750 their help in the identification of neuroblastoma diagnosis/relapse pairs and V. Bernard for pairs  
751 validation. We thank V. Saint-André for scientific discussion, J. Maliash-Planchon and the Unité  
752 de Génétique Somatique for preparation of patient samples. We thank Pr. Figarella-Branger (BB-  
753 033-00097, CRB AP-HM, CRB TBM, AC-2013-1786), M. Clapisson (CRB Centre Léon Bérard,  
754 AC-2008-101), Dr Minckes, Dr Blanc-Fournier and N. Rousseau (CHU, Tumorothèque - Caen  
755 Basse-Normandie) for providing tumor patient samples.

756

## 757 **Author information**

### 758 **Contributions**

759 V.B. and I.J.-L. conceived the study, analyzed the data and wrote the manuscript. V.B.  
760 coordinated bioinformatics analysis and I.J.-L. coordinated the whole study. C.L. performed *in*  
761 *vitro* experiments and all ChIP experiments and participated in the study design. A.P. generated  
762 and analyzed the doxycycline-inducible anti-*PHOX2B* shRNA cell lines. S.D. performed the  
763 single cell analysis and study of chemotherapeutic agents. C.P.-E. performed the *in vivo*  
764 experiments and contributed *in vitro* experiments. V.R. performed all sequencing experiments.  
765 H.E. and S.T. provided hNCC cell lines and V.C. provided neuroblastoma cell lines. A.L.  
766 performed alignment of RNA-seq and ChIP-seq data. E.D.-D., B.G., D.S. and A.M.C. provided  
767 neuroblastoma PDXs. I.M. performed the reproducibility analysis. E.D. and B.D. generated the  
768 Biomark data. M.F.O. and T.G.P.G. generated lentiviral particles and provided help with  
769 lentiviral infections. S.B. coordinated and supervised sequencing experiments. G.S. participated  
770 in the study design and provided the in-house pairs of diagnosis/relapse samples with the help of  
771 E.L., G.P. and B.G. S.G.-L. participated in RNA-seq analysis. E.B. provided computational  
772 infrastructure and data storage. H.R. and T.D. provided expertise in sympathetic nervous  
773 development and transcription factors. I.J.-L and O.D. provided laboratory infrastructure. I.J.-L,  
774 V.B. and O.D. provided financial support. All authors read and approved the final manuscript.

775

### 776 **Competing financial interests**

777 The authors declare no competing financial interests.

778

779 **Corresponding authors**

780 Correspondence to:

781

782 • Valentina Boeva: [valentina.boeva@inserm.fr](mailto:valentina.boeva@inserm.fr)

783 • Isabelle Janoueix-Lerosey: [janoueix@curie.fr](mailto:janoueix@curie.fr)

784

785

786

787

788

789

790

791

792 **Extended data figures and tables**

793

794 **Supplementary Table 1:** *MYCN*, *ALK* and *PHOX2B* status of neuroblastoma cell lines and  
795 PDXs. Amp., amplification; Non amp., non amplified; WT, wild-type. NA: not available.

796 \* As determined by Sanger sequencing of exons 23 and 25.

797 <sup>□</sup> *MYCN* locus: 5 copies; *MYC* locus: 7 copies; *ALK* locus: 7 copies (from Control-FREEC  
798 analysis)

799 <sup>#</sup> In frame deletion in the second PolyAlanine track; functional change unknown.

800

801 **Supplementary Table 2:** Patient clinical data.

802

803 **Supplementary Table 3:** Characteristics of neuroblastoma and hNCC super-enhancers. Group I:  
804 all neuroblastoma cell lines with the exception of SH-EP, GIMEN, *GICAN*, SK-N-AS, SJNB12,  
805 SK-N-SH and CHP-212; Group II: SH-EP, GIMEN and *GICAN*.

806

807 **Supplementary Table 4:** Supervised analysis of SE scores according to *MYCN* status.

808

809 **Supplementary Table 5:** Supervised analysis of SE scores according to ALK status.

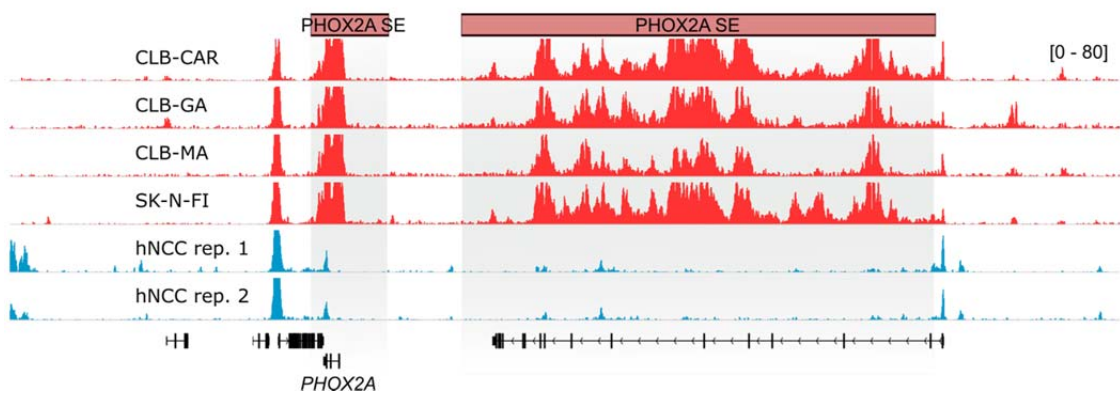
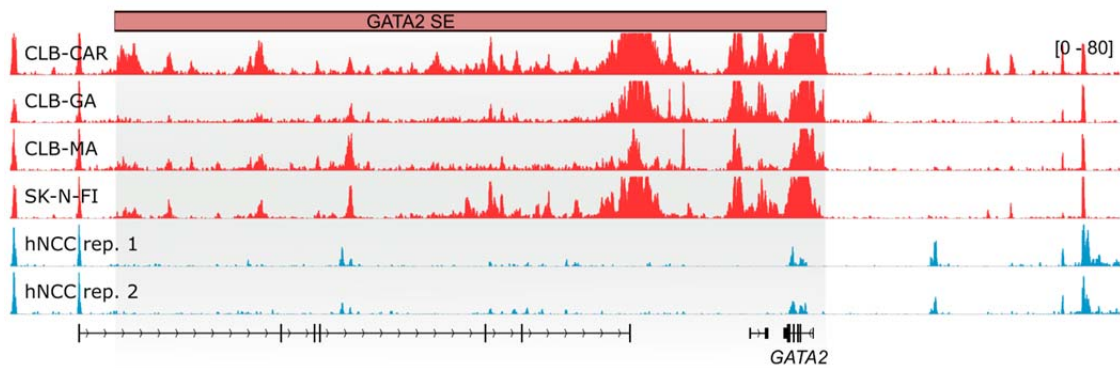
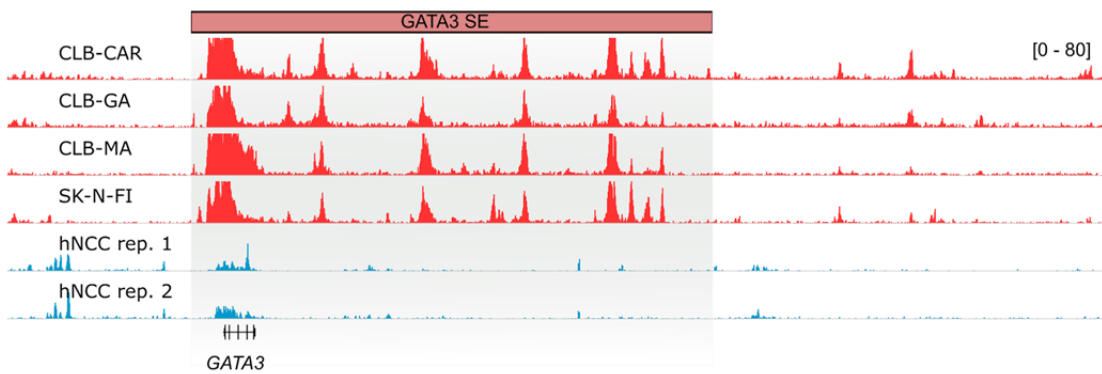
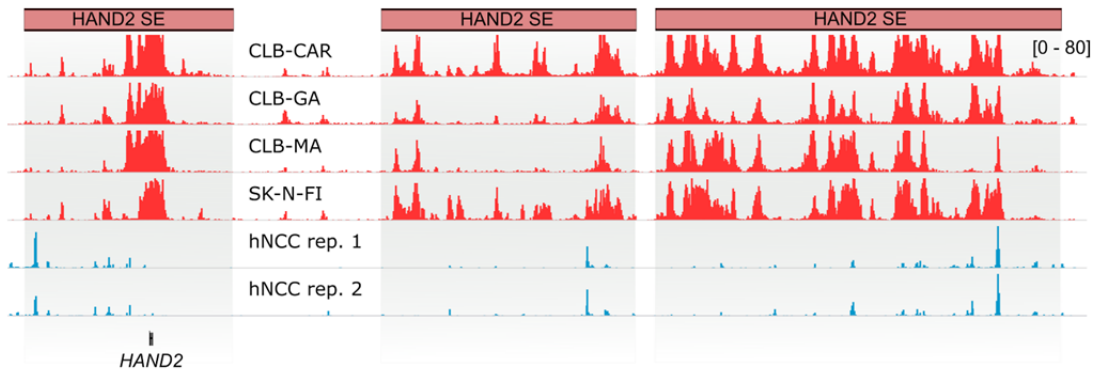
810

811 **Supplementary Table 6:** Raw Ct values measured for housekeeping genes (GAPDH, ACTG1,  
812 ACTB, RPL15) and TFs of modules 1 and 2 for single cells of the SK-N-AS, SH-EP, SH-SY5Y  
813 and SK-N-SH cell lines using the Fluidigm Biomark HD.

814

815





817 **Supplementary Figure 1:** Tracks for ChIP-seq profiles of H3K27ac at *HAND2*, *GATA3*,  
818 *GATA2*, and *PHOX2A* SEs.

819

820

821

822

823

824

825

826

827

828

829

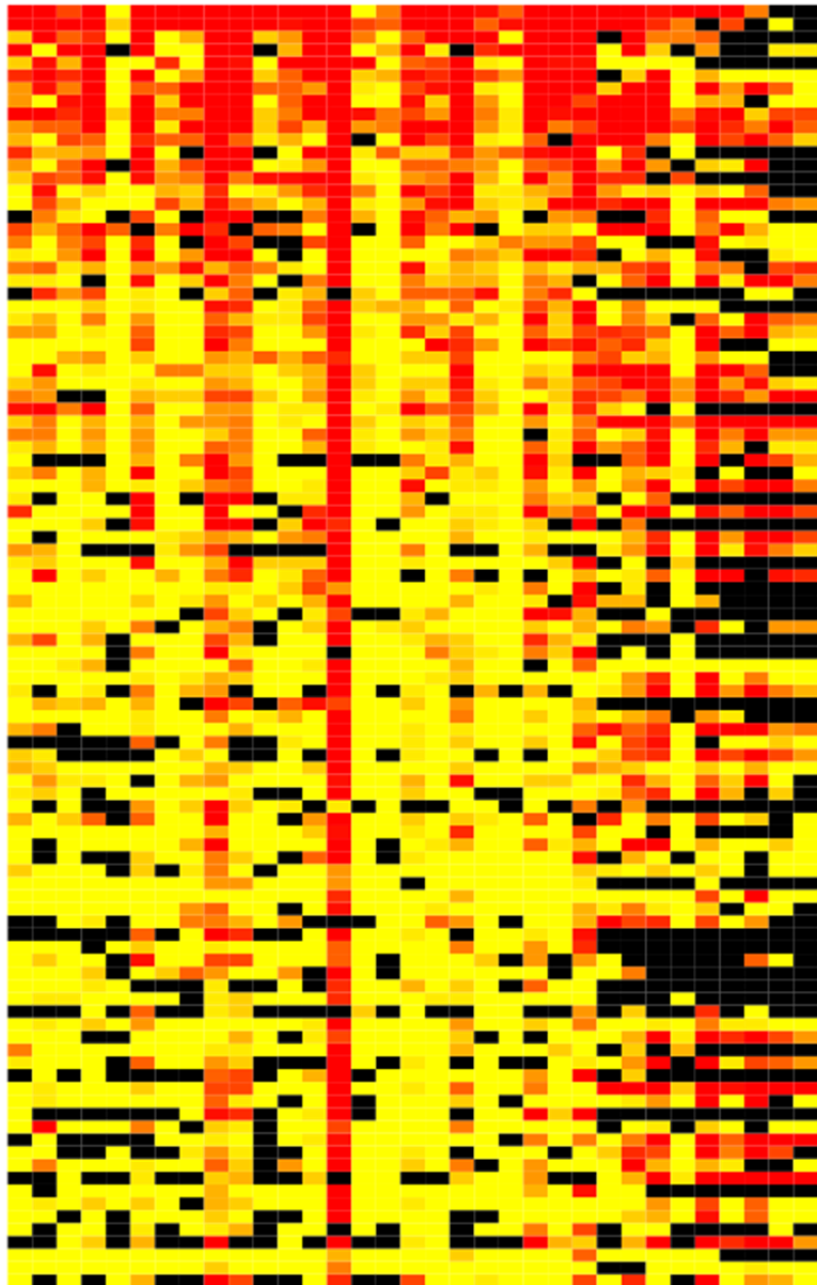
830

831

832

833

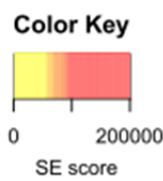
**a**



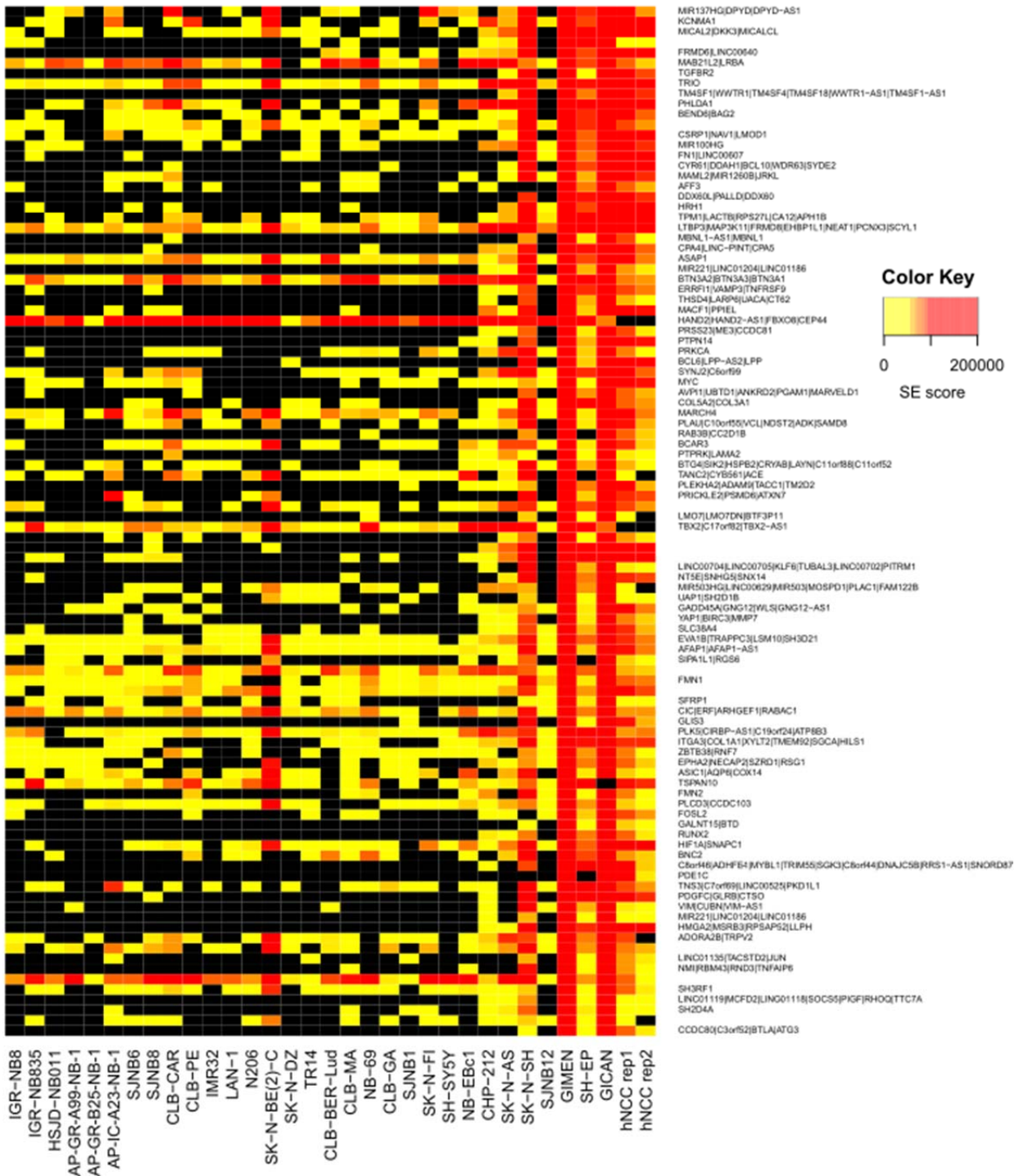
IGR-NB8  
IGR-NB835  
HSJD-NB011  
MAP-GR-A99-NB-1  
MAP-GR-B25-NB-1  
MAP-IC-A23-NB-1  
SJNB6  
SJNB8  
CLB-CAR  
CLB-PE  
IMR32  
LAN-1  
N206  
SK-N-BE(2)-C  
SK-N-DZ  
TR14  
CLB-BER-Lud  
CLB-MA  
NB-69  
CLB-GA  
SJNB1  
SK-N-FI  
SH-SY5Y  
NB-EBc1  
CHP-212  
SK-N-AS  
SK-N-SH  
SJNB12  
GIMEN  
SH-EP  
GICAN  
hNCC rep1  
hNCC rep2

**Associated genes**

HAND2|HAND2-AS1|FBXO8|CEP44  
GSE1|MR509|GINS2  
SLIT3|FBLN1|MR21B-2  
DLK1|BEGAIN|RTL1|MEG8|MEG9|MEG33|INO0523|SLC25A47  
EML5|TTC9|KCNK10  
MAML3  
TCF4  
MAG21L2|LRBA  
GATA2|GATA2-AS1|RLVBL1|DNAJB8|DNAJB8-AS1|EEFSEC  
UNC5C|BMPR1B  
PHOX2B|LMCH1|INO0082  
GATA3|GATA3-AS1|TAF3  
BTN3A2|BTN3A3|BTN3A1  
KIF26B|SMYD3  
PRR34-AS1|MRLET7B|PRR34  
PER3  
MWRCH4  
ALK  
PHOX2A|CLPB|NUMA1|LRTOMT|PDE2A  
KLF7  
TENM4  
HAND2|HAND2-AS1|HMGB2|SAP30  
TBX2|C17orf82|TBX2-AS1  
IGFBP4|TNS4  
KIF26A|TMEM179  
LTBP3|MAP3K11|FRMD8|EBHP1|1|NEAT1|PCNO3|SCYL1  
C1C|ERF|ARHGEF1|RABAC1  
JRAJD1C-AS1  
STRAF6|CCDC33|SLR2|SLR  
ASAP1  
FAM155A  
MCF2|C2orf61|TTC7A|EPCAM  
ZNF608  
TP53|11|TSPAN18  
TSPAN10  
CHRNA3|CHRNA4|CHRNA5|CRABP1|CIB2|REB2|ADAMTS1|SH2D7|WDR61  
ARHGAP4|AVPR2  
EXOC4  
VEGFA  
RBM20|GLT1D1|ADQRD1|TMEM132C  
BEND5|ELAVL4|AGBL4  
RBM20|GPM  
ICA1|GLO1|INXPH1|PRA3|MO6|UMAD1  
MAG21L1|NBEA|RFC3  
PLK5|CRBP-AS1|C19orf24|ATP8B3  
LINC00578  
NOL4L  
NFIB  
FAM102A|FAM129B  
ZFP96L2  
BCOR  
SEC24D|SYNPO2  
INSM2  
HAND1  
SSH2  
COL3A1|GULP1  
ASTN2  
BCOR  
CADM1  
SYT1  
PK3R1  
MYT1L|LINC01250  
SESN3  
IERSL  
ZNF423  
DENND3  
HAND2|HAND2-AS1  
TRIO  
HIF1A|SNAPC1  
ADORA2B|TRPV2  
NCOA7  
TPM1|ACTB|RP527|LCA12|APH1B  
NHSL2|CITED1|RGA04|ERCC6L  
LGALS3BP  
ATF7|TNS2|IGFBP6|NPF|FRAG  
CPFB4  
MR137HG|DPYD|DPYD-AS1  
CBX1|SP2  
DCP2|MCC  
POLM5|BMPR1B



**b**

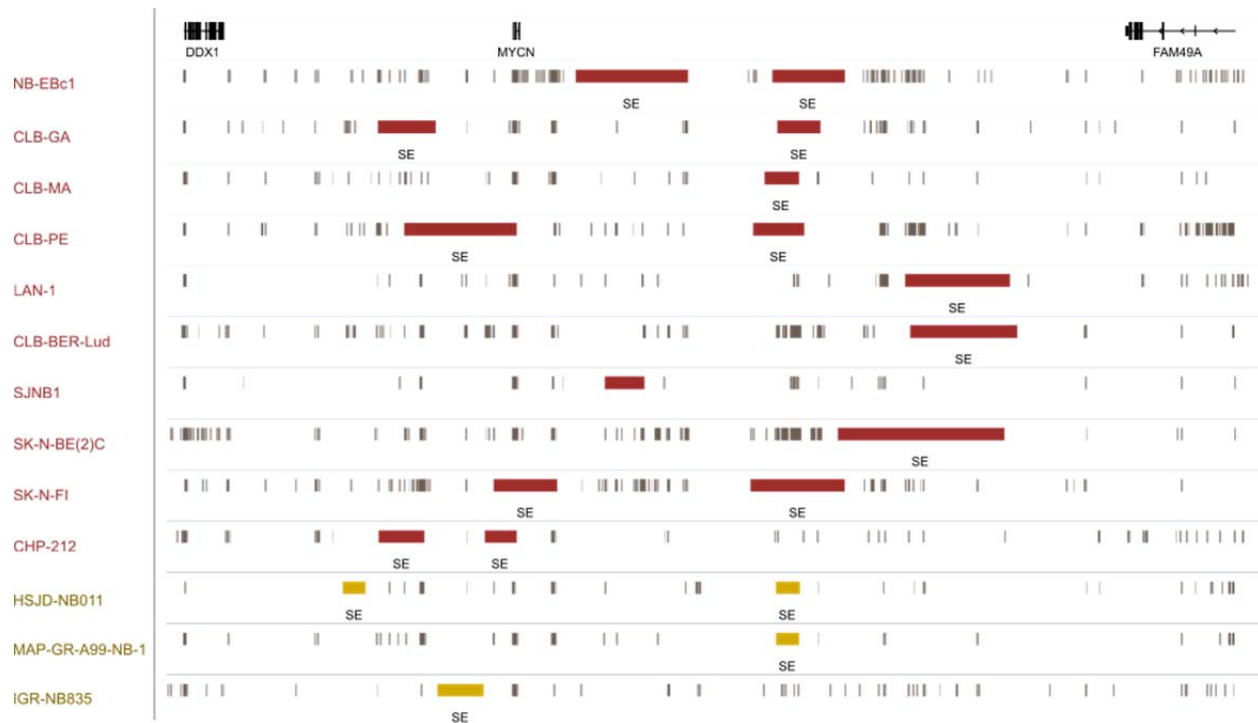


835

836 **Supplementary Figure 2:** Heatmap of the SE scores for the 6 PDX, 25 NB cell lines and hNCC

837 cells: top SEs of group I (a); top SEs of group II (b); SE is not detected (black).

838




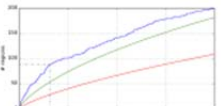

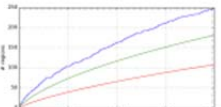

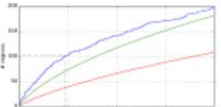

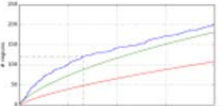

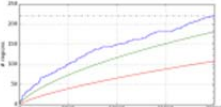

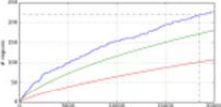

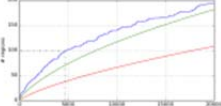
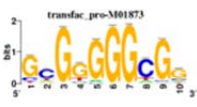
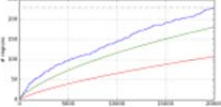
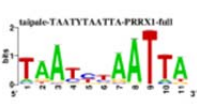
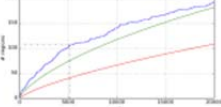

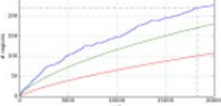

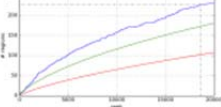
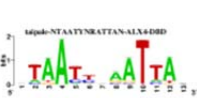
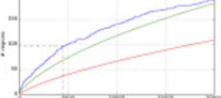
839

840

841

842 **Supplementary Figure 3:** Locations of SE regions predicted for the *MYCN* locus; SEs in NB  
 843 cell lines (red); SEs in PDX (yellow); typical enhancers and active promoters (grey).

844

#	Feature	NES	Logo	Recovery Curve
1.	TAAYYNAATTA-PROP1-full	4.21		
2.	PGAM2	3.98		
3.	TAATYYAATTA-PHOX2B-DBD	3.98		
4.	GATA1, GATA2, GATA3, GATA4, GATA5, GATA6	3.94		
5.	ZCCHC14	3.85		
6.	WT1	3.84		
7.	TAATYYAATTA-PHOX2A-DBD	3.76		
8.	EGR1	3.75		
9.	TAATYTAATTA-PRRX1-full	3.74		
10.	SP1:SP3	3.72		
11.	SP4	3.72		
12.	ALX4	3.71		

845

846 **Supplementary Figure 4:** i-cis Target summary (database v3.0) on H3K27ac peak valleys of the  
847 top 100 strongest SEs identified in group I. NES, Normalized enrichment score. NES threshold

848 3.7. NES and recovery curves are explained at the i-cisTarget website:

849 <https://gbiomed.kuleuven.be/apps/lcb/i-cisTarget/> .

850

851

852

853

854

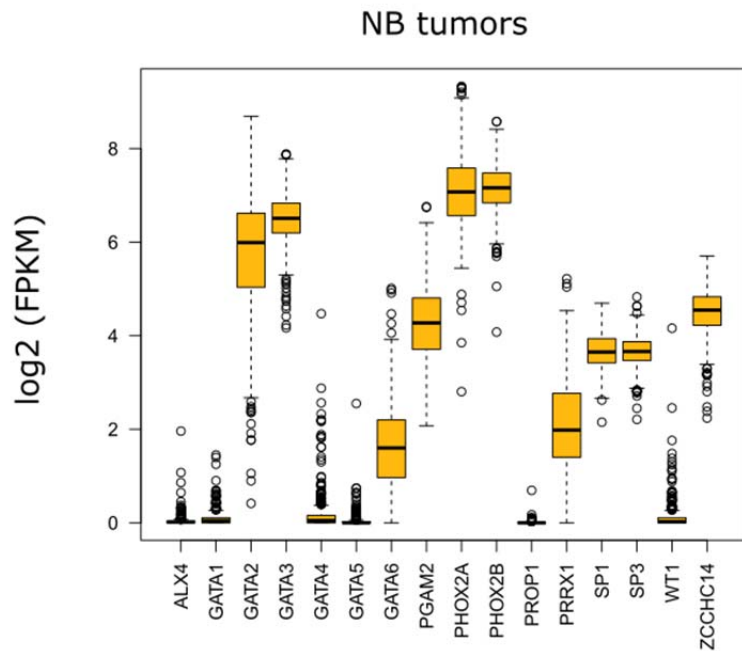
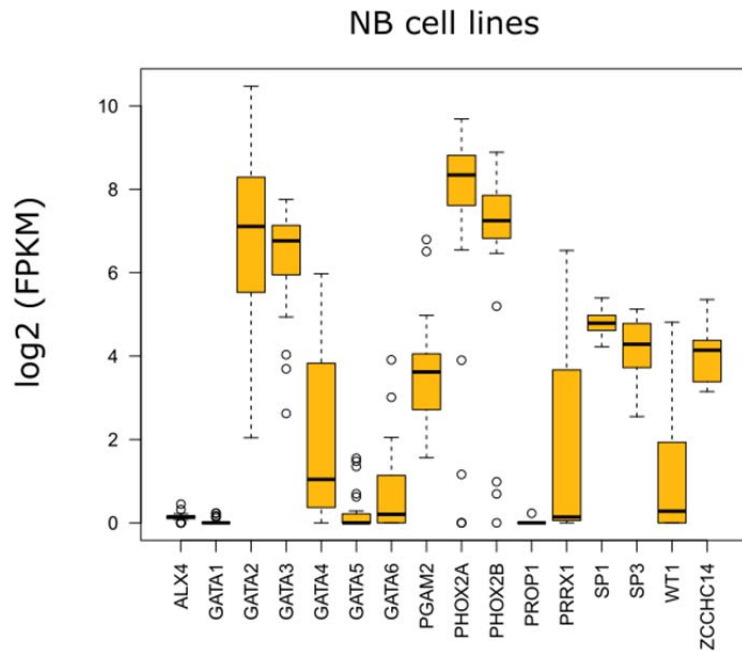
855

856

857

858

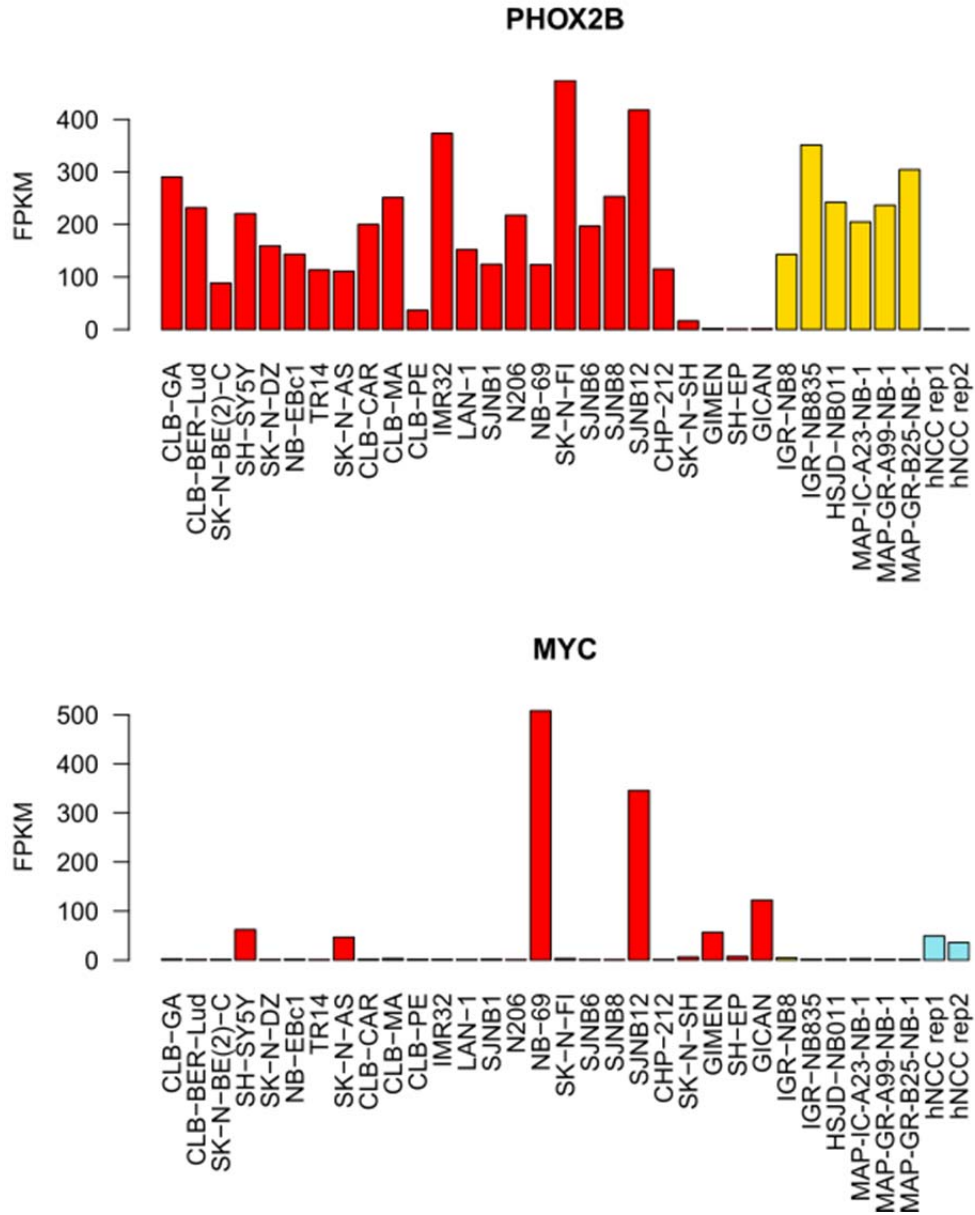
859



860

861 **Supplementary Figure 5:** Log<sub>2</sub> FPKM expression values for genes coding for TFs whose  
 862 binding motifs are enriched in valleys of H3K27ac peaks of the top 100 strongest SEs identified  
 863 in group I, in neuroblastoma (NB) cell lines (our data) and NB primary tumors (498 tumors,  
 864 dataset GSE49711). The box represents the middle 50% of values; the black line inside the box  
 865 indicates the median.

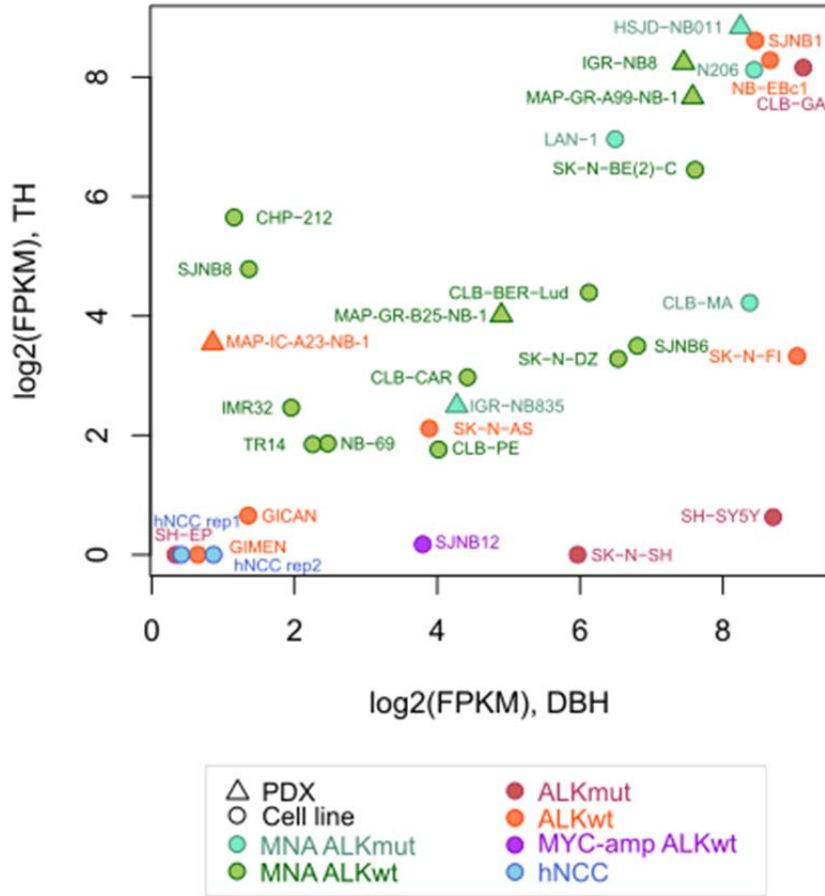




866  
 867  
 868  
 869  
 870

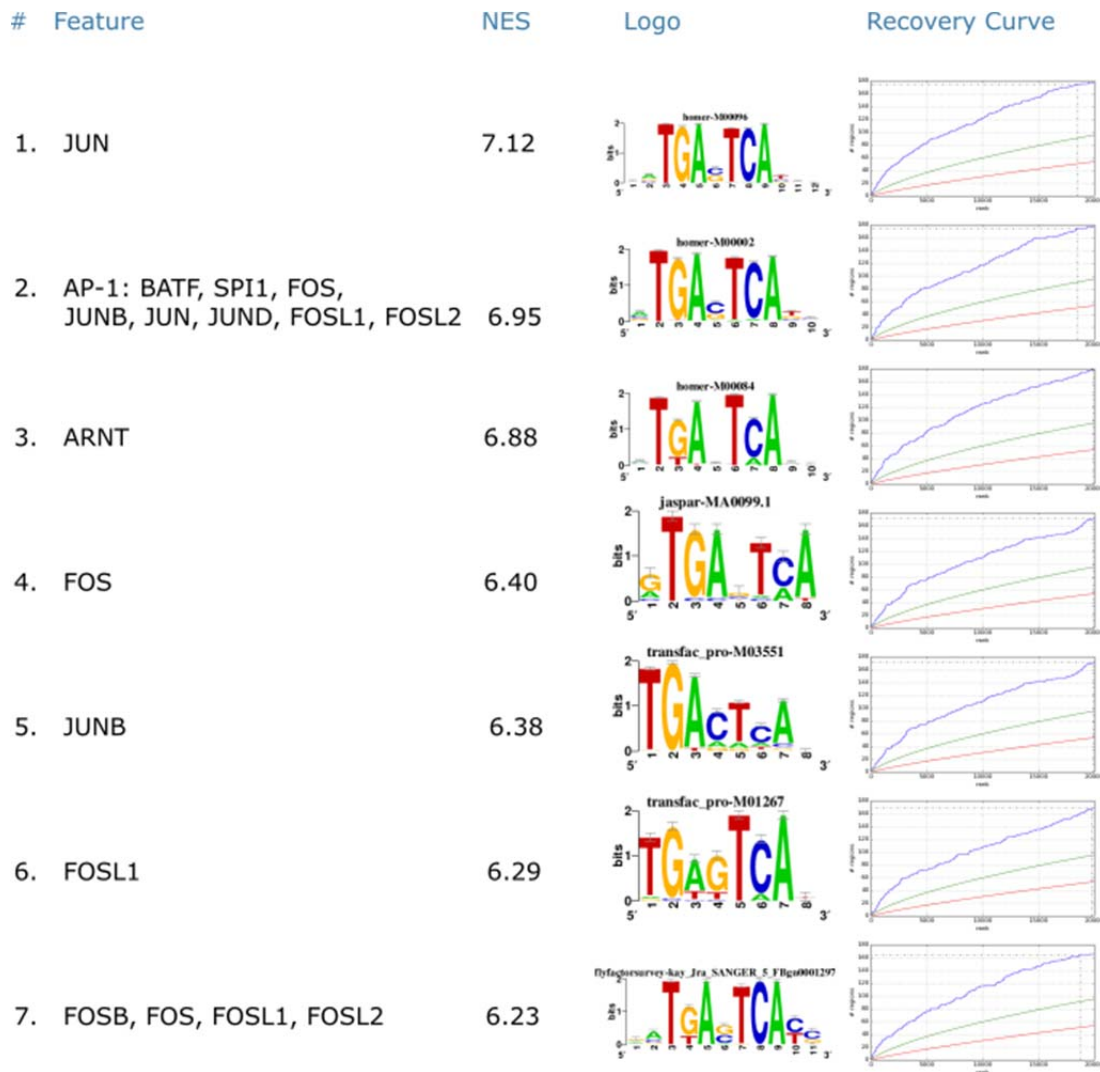
**Supplementary Figure 6:** *PHOX2B* and *MYC* expression levels measured by RNA-seq in neuroblastoma cell lines (red), PDX (yellow) and hNCC lines (blue).

871  
872



873  
874  
875  
876  
877  
878  
879  
880  
881  
882  
883

**Supplementary Figure 7:** Log2 FPKM expression values of *DBH* and *TH* in hNCC and neuroblastoma cell lines and PDX measured by RNA-seq.



884

885

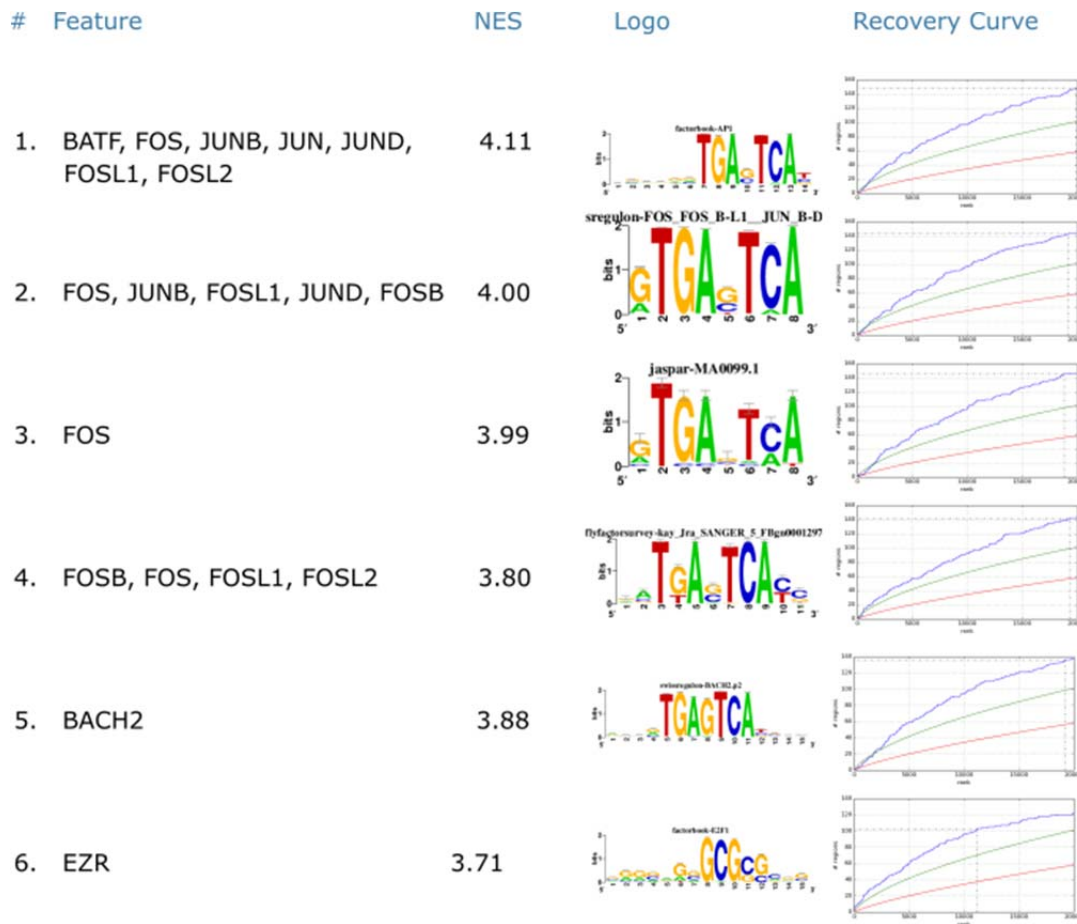
886

887 **Supplementary Figure 8:** i-cis Target summary (database v3.0) on H3K27ac peak valleys of the

888 top 100 strongest SEs identified in group II. NES, Normalized enrichment score. NES threshold

889 6.2. NES and recovery curves are explained at the i-cisTarget website:

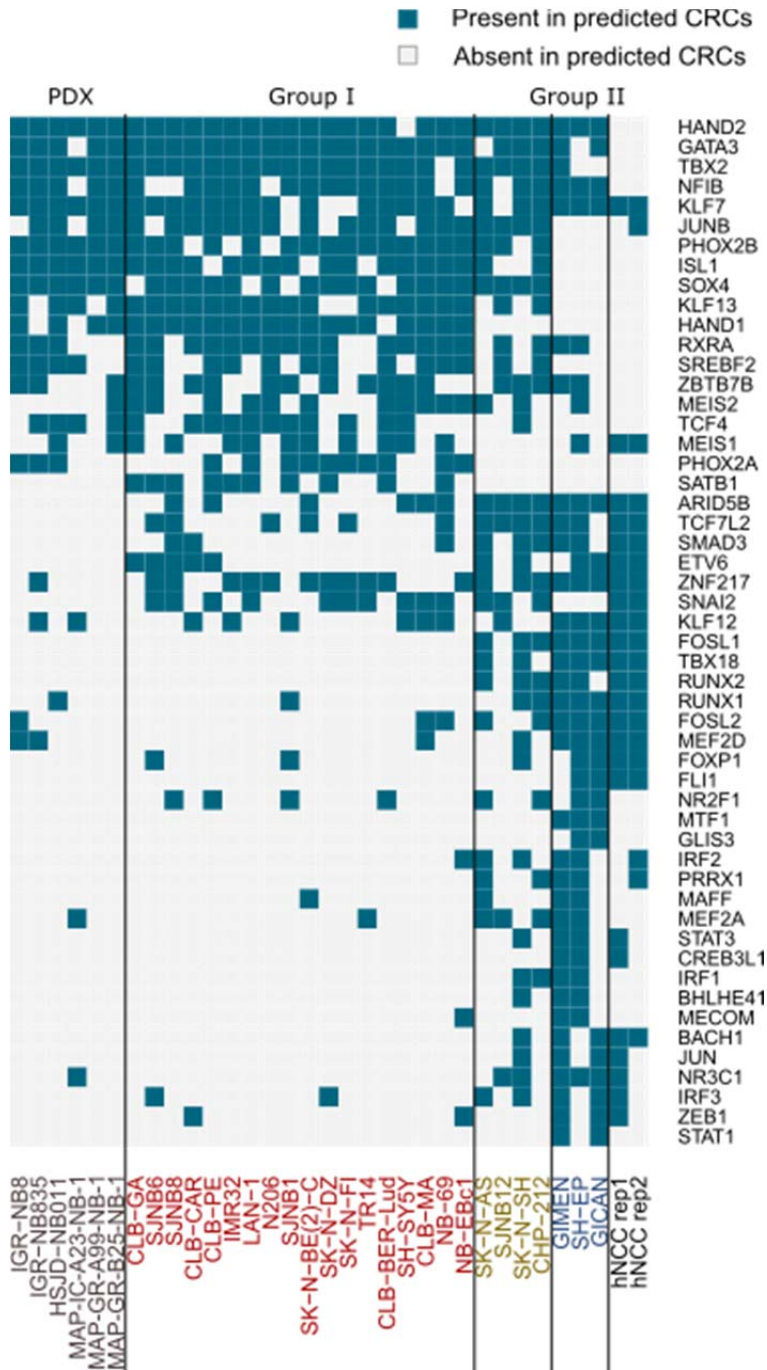
890 <https://gbiomed.kuleuven.be/apps/lcb/i-cisTarget/>.



891  
892 **Supplementary Figure 9:** i-cis Target summary (database v3.0) on H3K27ac peak valleys of the  
893 top 100 strongest SEs identified in hNCC. NES, Normalized enrichment score. NES threshold  
894 3.7. AUC threshold 0.015. NES and recovery curves are explained at the i-cisTarget website:  
895 <https://gbiomed.kuleuven.be/apps/lcb/i-cisTarget/> .

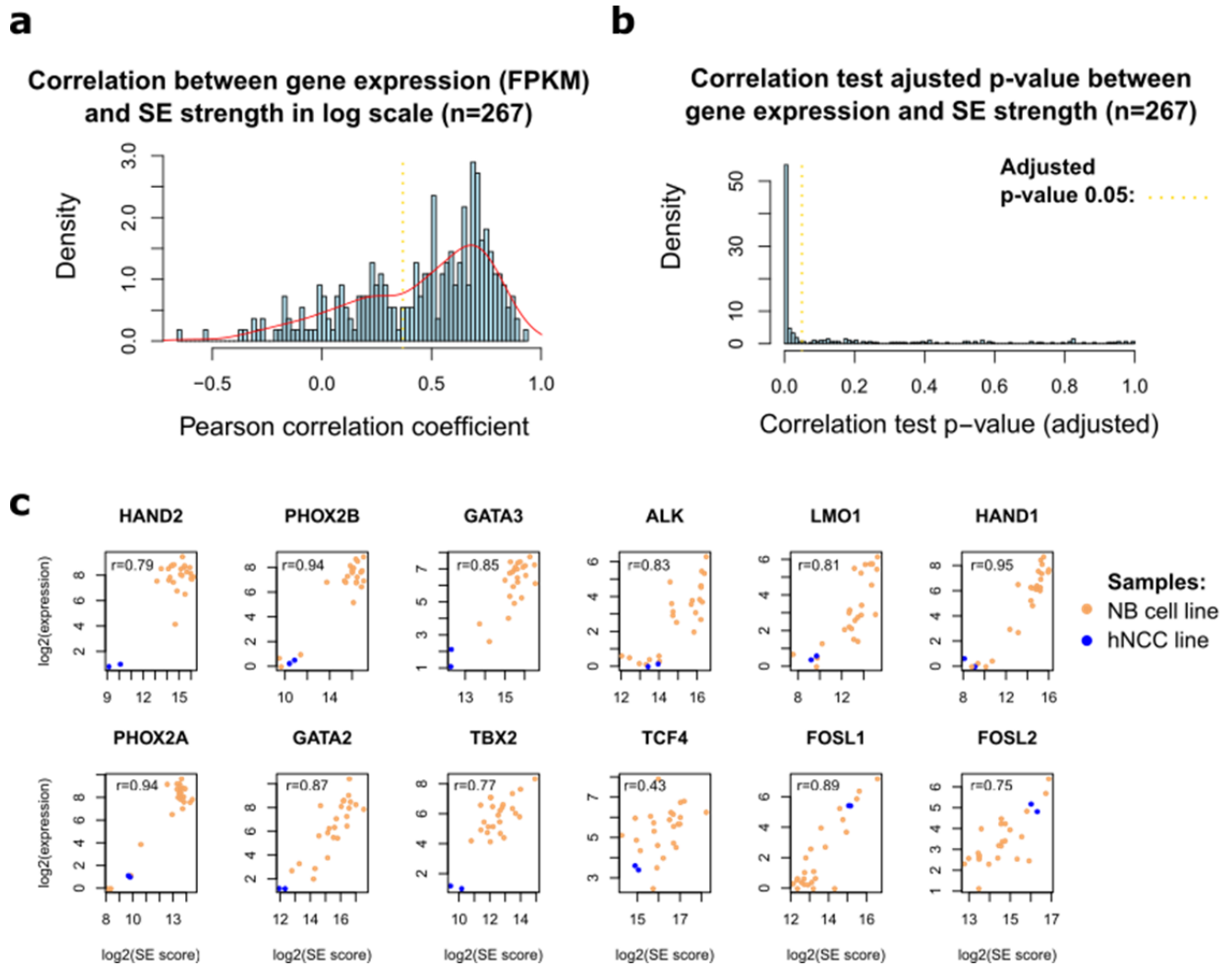
896  
897  
898

899  
900  
901



902  
903  
904  
905

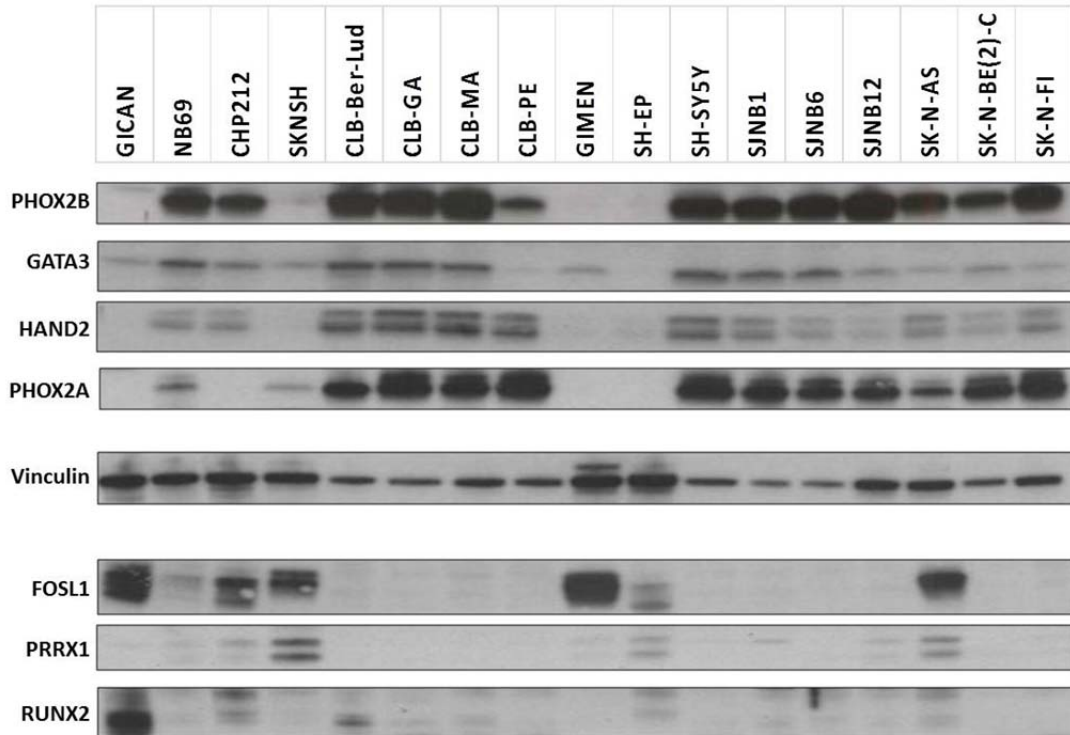
**Supplementary Figure 10:** TFs predicted to participate in CRCs in the two groups of neuroblastoma cell lines, and the primary hNCC.



906  
 907  
 908  
 909  
 910  
 911  
 912  
 913  
 914  
 915  
 916  
 917  
 918

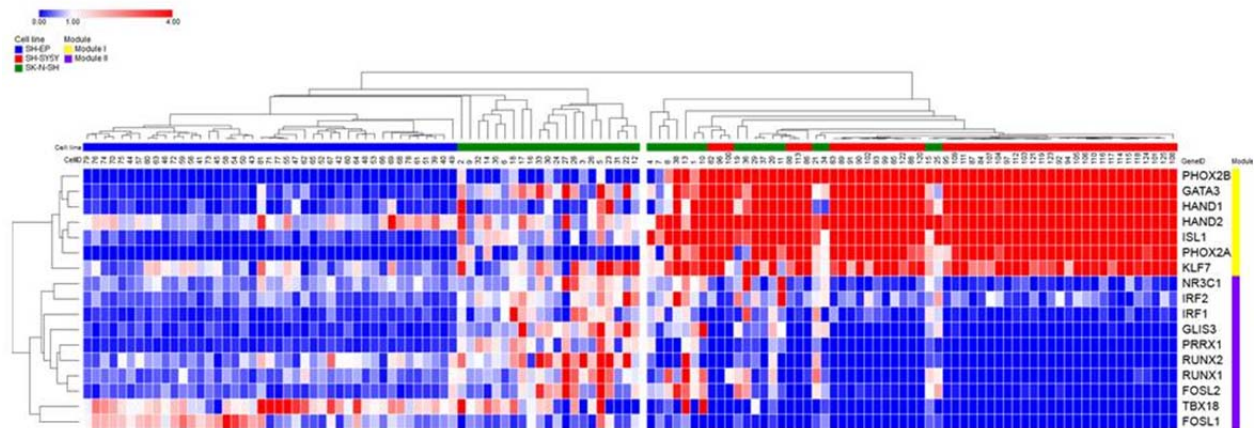
**Supplementary Figure 11:** Gene expression linearly correlates with SE score (in log scale). **a**, Pearson correlation coefficients were calculated for 267 SE regions corresponding to only one gene and detected in at least 2 neuroblastoma samples. Pearson correlation one-sided permutation tests were performed on the set of 25 neuroblastoma cell lines and 2 hNCC samples; **p-values adjusted with the FDR method.** **b**, Distribution of corresponding adjusted p-values for 267 SE regions. **c**, Examples of correlation between SE score and expression of particular genes. Orange: neuroblastoma cell lines; blue: hNCC samples.

919  
920



921  
922  
923  
924  
925  
926  
927  
928  
929  
930  
931  
932  
933

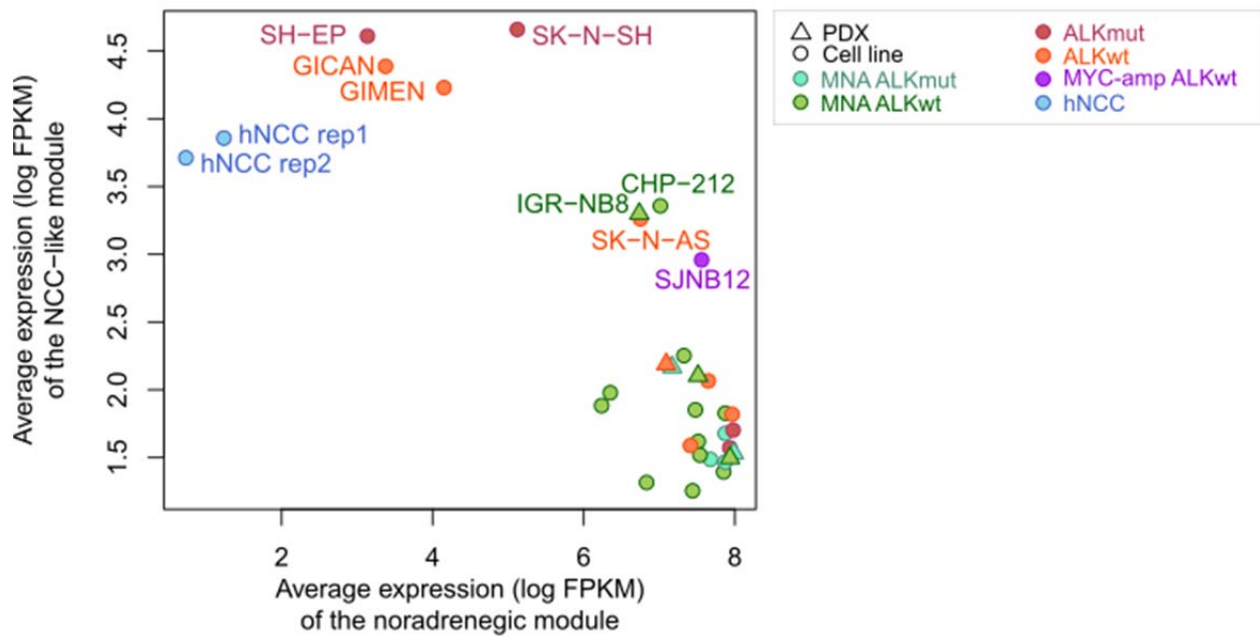
**Supplementary Figure 12:** Western blot analysis of PHOX2B, GATA3 (CST #5852, D13C9), HAND2 (sc-9409), PHOX2A (sc-8978), FOSL1 (sc-28310), PRRX1 (Sigma HPA051084), RUNX2 (sc-101145) and vinculin in a panel of neuroblastoma cell lines. All antibodies were used at 1:500 except the GATA3 antibody used at 1:1000.



934  
 935 **Supplementary Figure 13:** Clustering of SK-N-SH, SH-EP and SH-SY-5Y single cells  
 936 analyzed by RT-q-PCR for the expression of TFs of modules 1 and 2. The first group of cells  
 937 includes all SH-EP cells as well as some cells of the SK-N-SH cell line; a second group includes  
 938 all SH-SY5Y cells as well as cells of the SK-N-SH cell line. RT-q-PCR data were normalized to  
 939 the SK-N-SH cell line population for the three cell lines using the geometric mean of the four  
 940 housekeeping genes.

941  
 942  
 943  
 944  
 945  
 946  
 947  
 948  
 949  
 950  
 951  
 952  
 953  
 954





955

956 **Supplementary Figure 14:** Expression of modules 1 and 2 in neuroblastoma cell lines and

957 PDXs. Average is calculated for log<sub>2</sub> FPKM values.

958

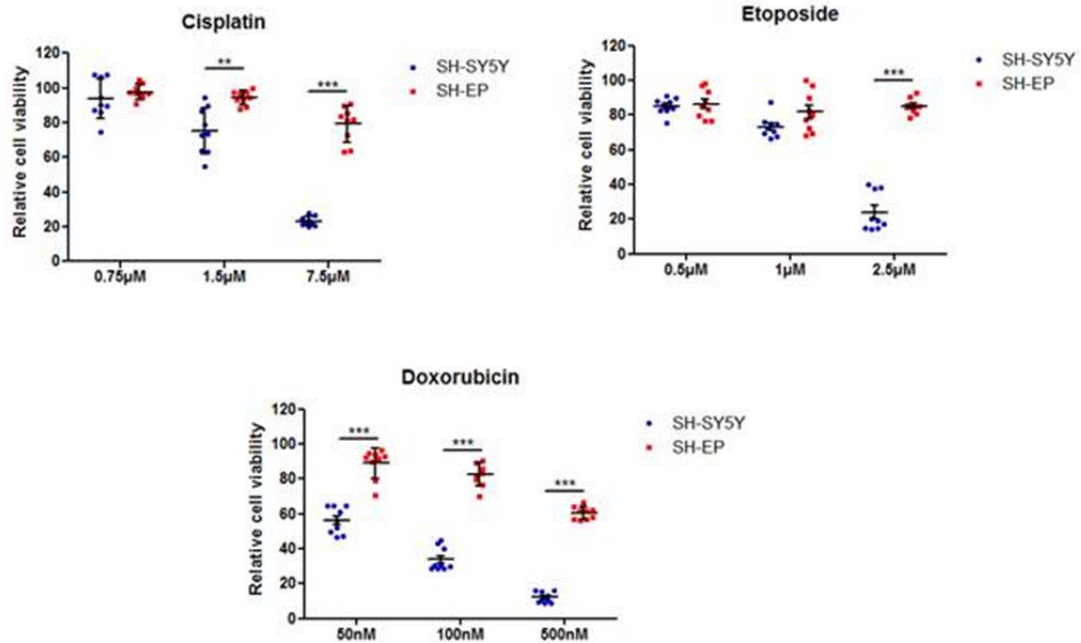
959

960

961

962

963



964

965

966 **Supplementary Figure 15:** NCC-like SH-EP cells are more resistant to chemotherapy than  
 967 noradrenergic SH-SY5Y cells (n=9 technical replicates per condition; P values were determined  
 968 via two-tailed unpaired Welch's t-test (\*\*\*: p<0.001)).

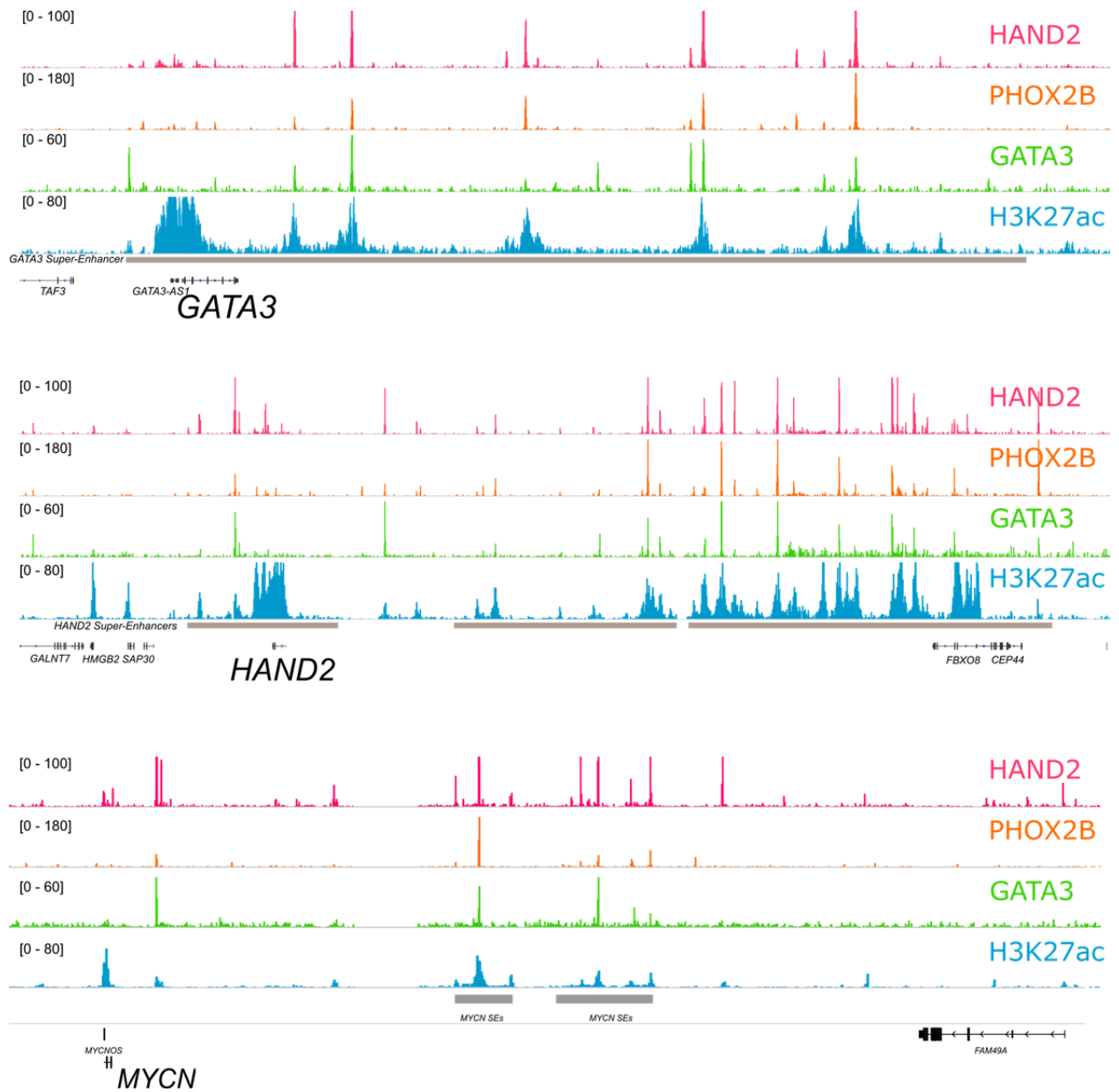
969

970

971

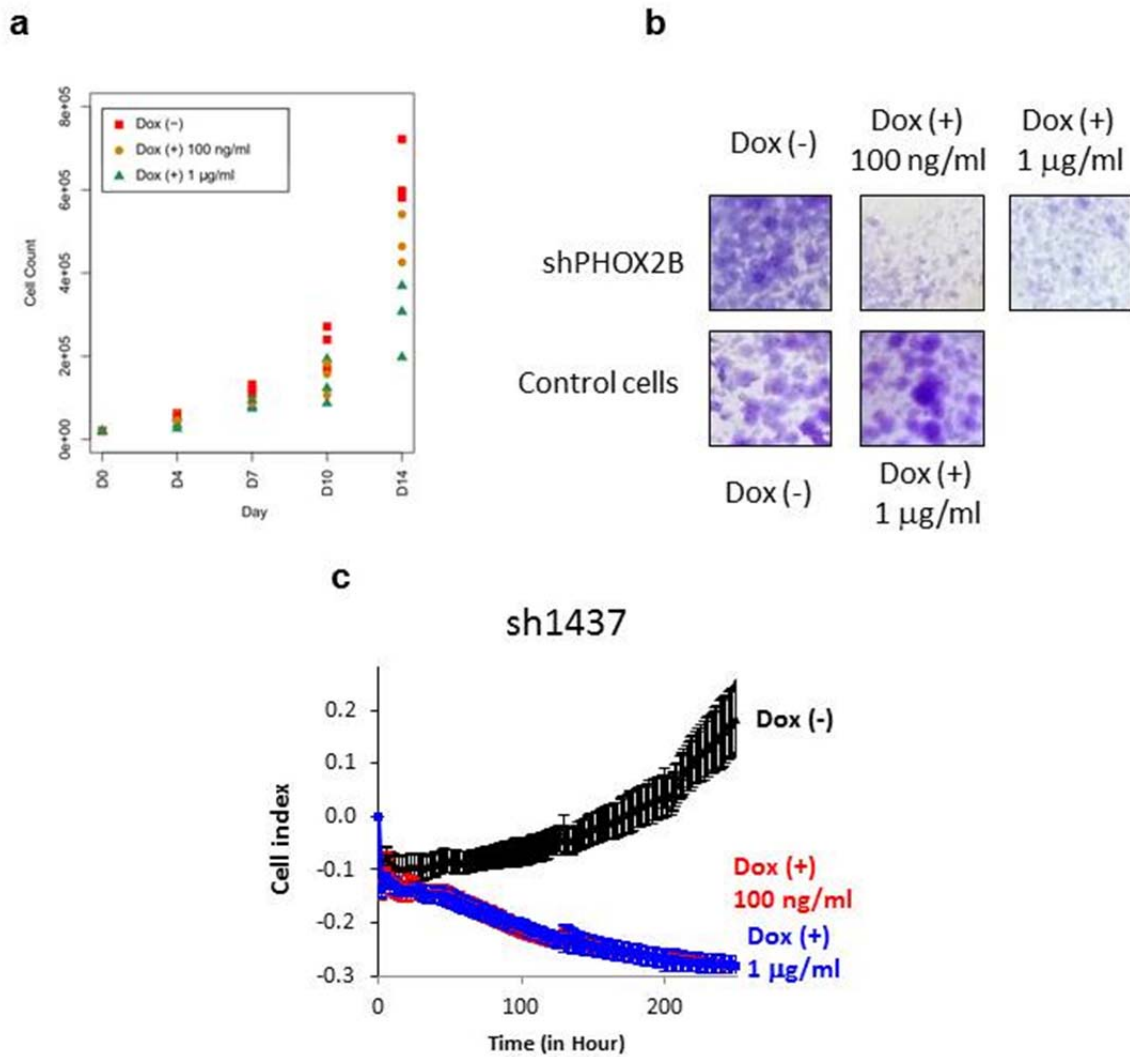
972

973



974  
 975  
 976  
 977  
 978  
 979  
 980  
 981  
 982

**Supplementary Figure 16:** Tracks for ChIP-seq profiles for PHOX2B, HAND2, GATA3 and H3K27ac binding at the *GATA3* (top), *HAND2* (middle) and *MYCN* (bottom) SEs in the CLB-GA cell line.



983

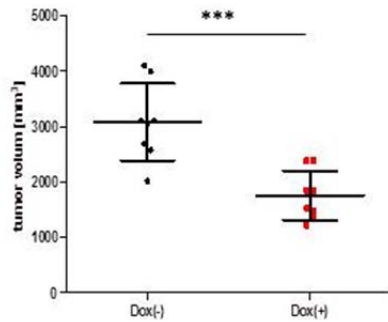
984

985 **Supplementary Figure 17: a**, Validation of xCELLigence™ results by cell counting for the  
 986 CLB-GA cell line infected with the sh1783 vector targeting PHOX2B.  $2 \times 10^4$  cells were plated in  
 987 24-well plates at day 0 in the absence or presence of doxycycline at 100 ng/ml or 1 µg/ml. The  
 988 number of living cells was counted at day 4, 7, 10 and 14. **b**, Decreased foci formation of CLB-  
 989 GA cells upon doxycycline-induced *PHOX2B* knockdown. Doxycycline at 1 µg/ml did not affect  
 990 growth of CLB-GA non-infected control cells. **c**, xCELLigence™ proliferation kinetics for the  
 991 SH-SY5Y cell line infected with the sh1437 vector targeting PHOX2B, respectively. Data shown  
 992 are the mean  $\pm$  s.d. of results obtained in the different conditions (n=5 technical replicates)

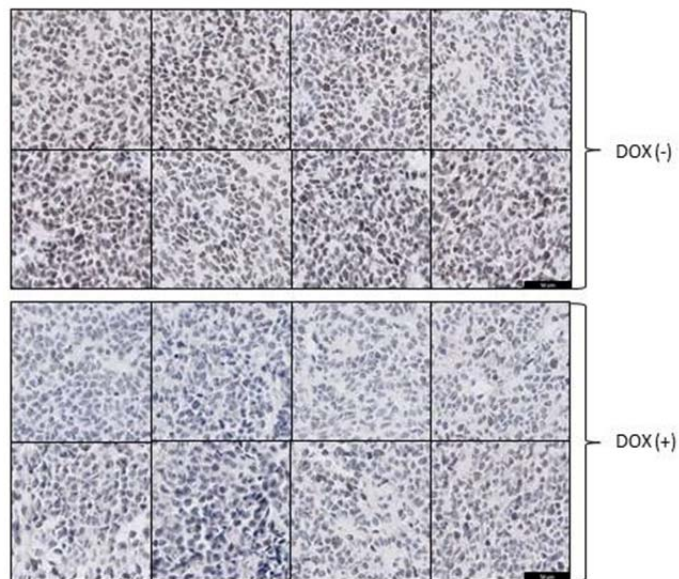
993

994

**a**



**b**



995

996

997

998 **Supplementary Figure 18: a**, Tumor volume of mouse xenografts of CLB-GA cells transduced

999 with sh1783 targeting PHOX2B after 11 days of treatment with sucrose alone (Dox(-)) or

1000 doxycycline and sucrose (Dox(+)). **b**, PHOX2B expression analyzed by immunohistochemistry

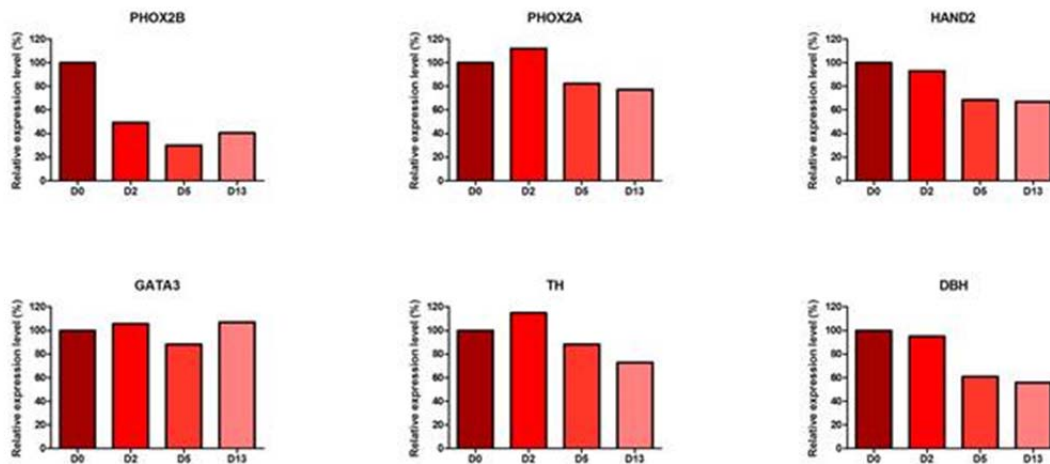
1001 (EPR14423-Abcam) in mouse xenografts of CLB-GA cells transduced with sh1783 targeting

1002 PHOX2B treated or not with doxycycline (DOX). Each panel corresponds to a different tumor

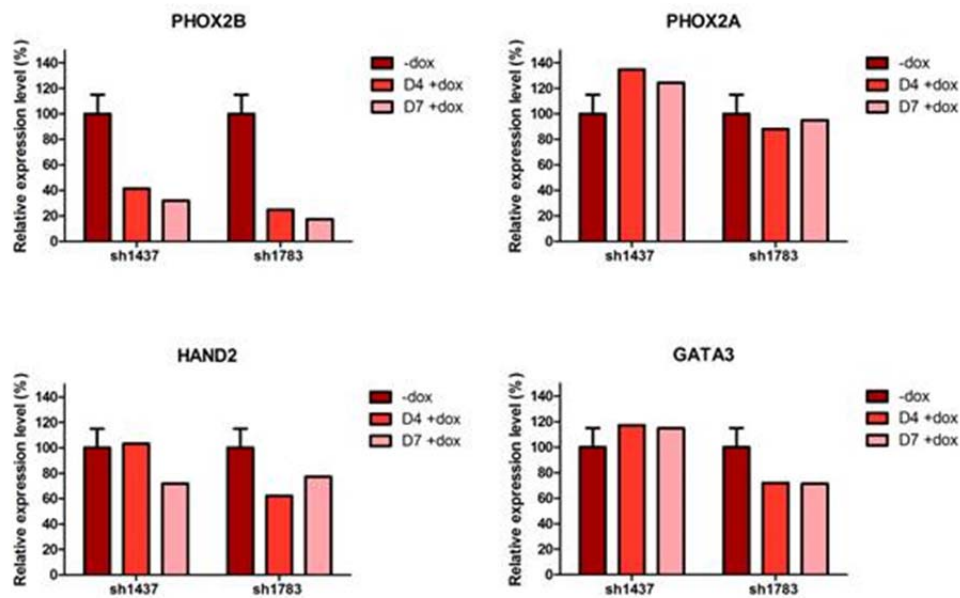
1003 (n=8 tumors in each group).

1004

**a**



**b**



1005

1006 **Supplementary Figure 19:** Impact of PHOX2B decrease on the expression profiles of CLB-GA

1007 and SH-SY5Y cells. **a**, RNA-seq was performed on CLB-GA cells transduced with sh1783

1008 targeting PHOX2B after 2, 5 and 13 days of doxycycline treatment and on untreated cells (D0).

1009 Expression levels (FPKM values) for each day are compared to the untreated cells (100%).

1010 PHOX2B knockdown resulted in a modest decrease of PHOX2A, HAND2, TH and DBH. No

1011 expression of the genes of the NCC-like module was detected in any of the conditions. **b**,

1012 Expression of genes of modules 1 and 2 was evaluated by RT-q-PCR on SH-SY5Y cells

1013 transduced with sh1437 or sh1783 targeting PHOX2B after 4 and 7 days of doxycycline  
1014 treatment and compared to untreated cells (100%). GAPDH was used as a reference gene. No  
1015 strong changes were observed following PHOX2B decrease. FOSL1, RUNX2 and PRRX1 were  
1016 not detected neither in the untreated condition nor after PHOX2B knockdown. TaqMan(r) Gene  
1017 Expression Assays (Thermo Fischer Scientific) used in this assays: GAPDH (4326317E),  
1018 PHOX2B (Hs00243679\_m1), HAND2 (Hs00232769\_m1), GATA3 (Hs00231122\_m1),  
1019 PHOX2A (Hs00605931\_mH), FOSL1 (Hs04187685\_m1), RUNX2 (Hs01047973\_m1), PRRX1  
1020 (Hs00246567\_m1).

1021

1022

1023

1024

1025

1026

1027

1028

1029

1030

1031

1032

1033

1034

1035

1036

1037

1038

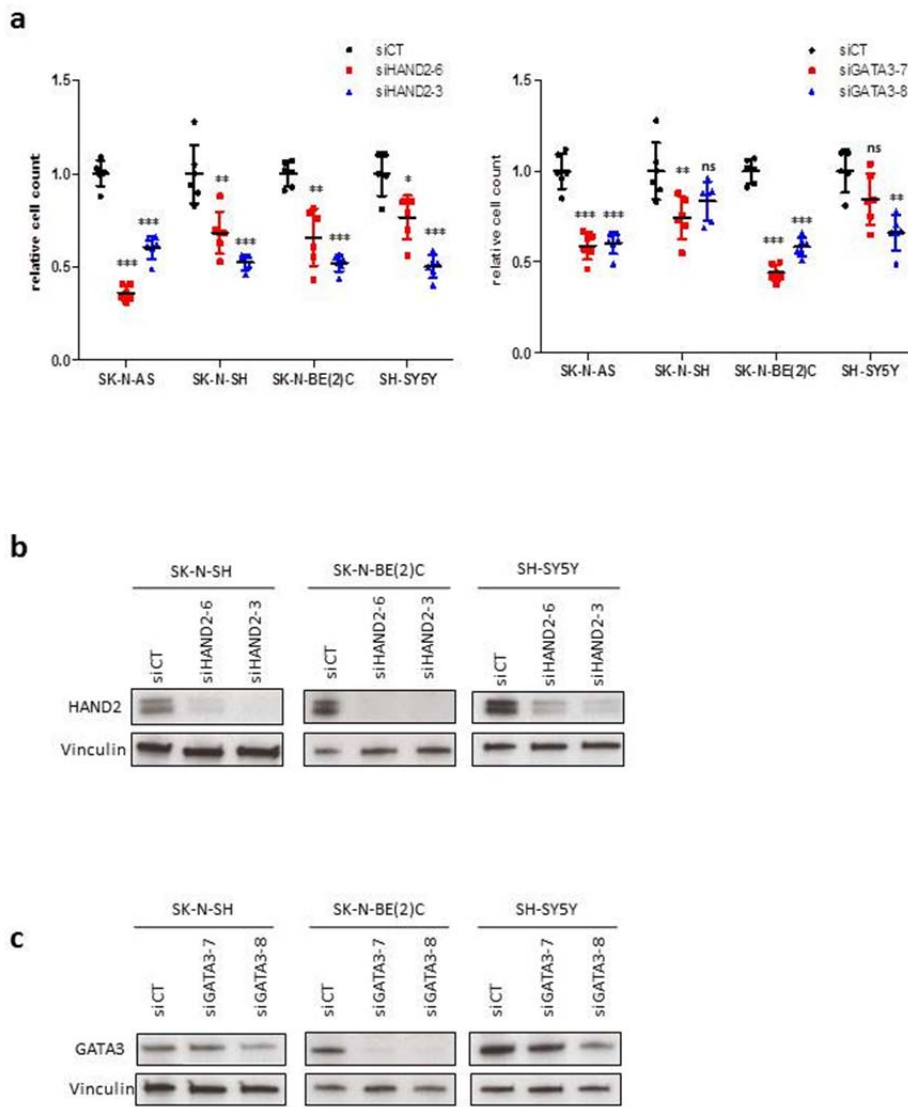
1039

1040

1041

1042

1043



1045

1046

1047

1048 **Supplementary Figure 20:** HAND2 and GATA3 knockdown impairs proliferation of SK-N-

1049 AS, SK-N-SH, SK-N-BE(2)C and SH-SY5Y cell lines. **a**, Cell counting of cells treated with

1050 siRNA targeting HAND2, GATA3 or with a control siRNA (at 3 days post-treatment for SK-N-

1051 BE(2)C, 5 days for SK-N-SH and 6 days for SK-N-AS and SH-SY5Y). (n=5 or 6 technical

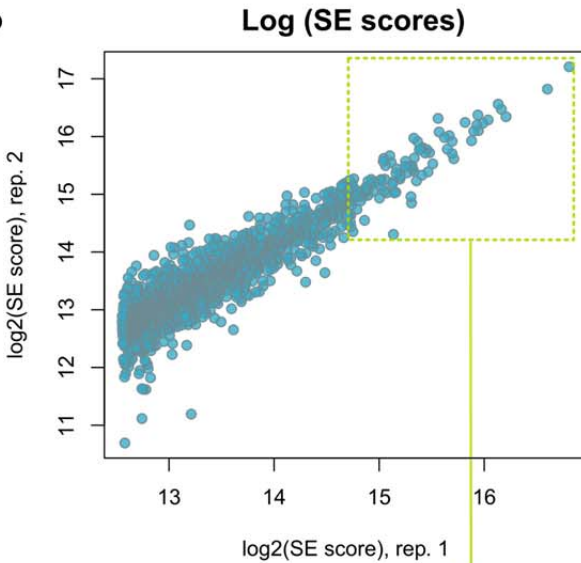
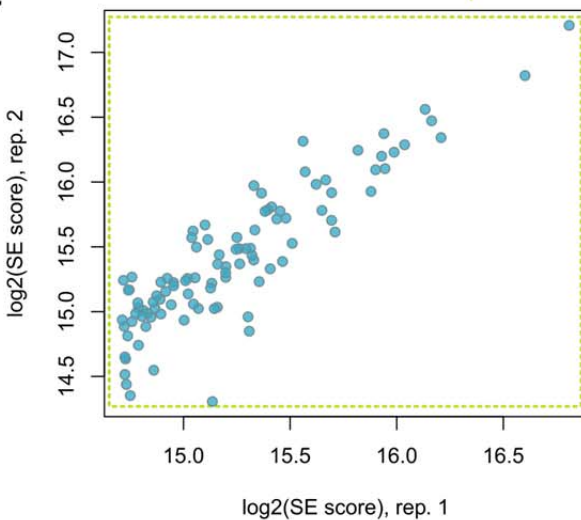
1052 replicates, mean +/- s.d.). P values were determined via two-tailed unpaired Welch's t-test (\*\*\*:

1053 p<0.001). **b and c**, Western blots for HAND2, GATA3, or vinculin.



**a**

	Proportion detected as SEs in rep. 2	Proportion detected as Enhancer in rep. 2
Top 100 SEs, rep. 1	100%	0%
Top 500 SEs, rep. 1	93%	6.6%
All SEs, rep. 1	75.6%	23.3%

**b****c****d**

	Pearson correlation coef. of SE log scores in rep. 1 and rep. 2	Spearman correlation coef. of SE log scores in rep. 1 and rep. 2
Top 100 SEs, rep. 1	0.90	0.86
Top 500 SEs, rep. 1	0.92	0.88
All SEs, rep. 1	0.93	0.90

1054

1055 **Supplementary Figure 21:** Reproducibility analysis of SE calling and score assessment. ChIP-1056 seq experiment for the H3K27ac mark was performed in duplicate for the CLB-GA cell line. **a**,1057 Proportion of active SEs from replicate 1 detected as SEs in replicate 2. **b, c**, Correlation

1058 between normalized values of SE scores in CLB-GA replicate 1 and 2, shown for all the SEs of  
1059 replicate 1 **(b)** and the top 100 SEs of replicate 1 **(c)**. **d**, Correlation coefficient for SEs scores  
1060 between replicate 1 and 2.

1061

1062

1063

1064

1065

1066

1067

1068

1069

1070

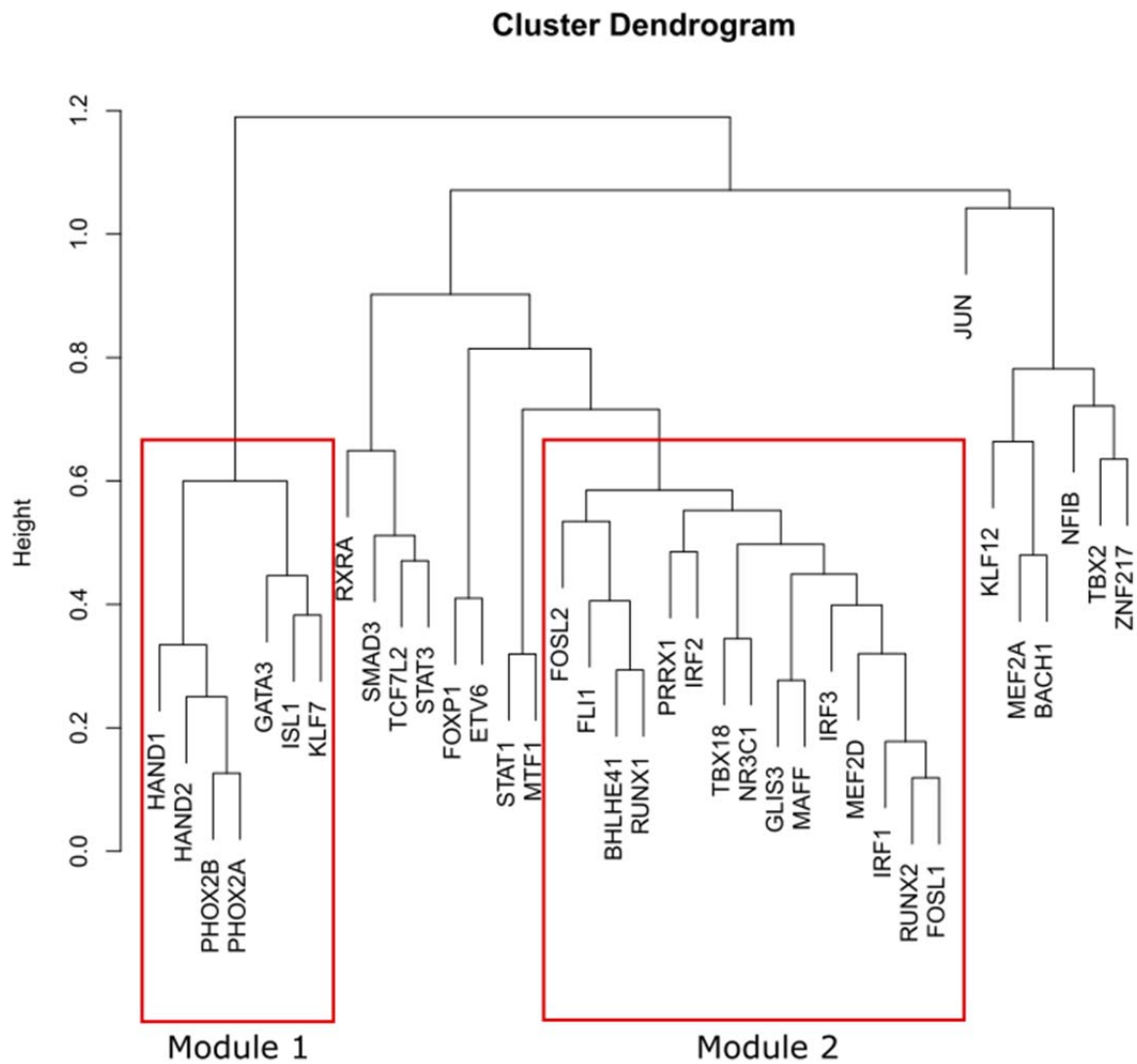
1071

1072

1073

1074

1075



1076

1077 **Supplementary Figure 22:** Clustering of 37 genes from CRCs of neuroblastoma group I and II  
 1078 based on their expression correlation in NB cell lines and PDX (R package ‘hclust’ with the  
 1079 McQuitty method). Two modules were defined.